ABSTRACT

Title of Thesis: INFORMATION CAPACITY AND POWER EFFICIENCY IN OPERATIONAL TRANSCONDUCTANCE AMPLIFIERS

Suvarcha Malhotra, Master of Science, 2003

Thesis directed by: Professor Pamela A. Abshire
Department of Electrical and Computer Engineering

Information capacity is a fundamental and quantitative bound on the ability of a physical system to communicate information. The capacity depends only on the physical properties of the channel, such as bandwidth, noise, and constraints on the signal values; it does not depend on specific tasks for which the channel may be used. Real analog systems possess intrinsic physical noise such as thermal noise and flicker noise and inevitably suffer degradation of information content. We investigate the information transmission and information-power efficiency of an Operational Transconductance Amplifier (OTA). We present empirical results for the information capacity of an integrated OTA and compare these results with our theoretical model. We notice a significant increase in information content if the system is operated in spectral regions with higher frequency and lower noise level.

INFORMATION CAPACITY AND POWER EFFICIENCY IN OPERATIONAL TRANSCONDUCTANCE AMPLIFIERS

by

Suvarcha Malhotra

Thesis submitted to the Faculty of the Graduate School of the
University of Maryland, College Park in partial fulfillment
of the requirements for the degree of
Master of Science
2003

Advisory Committee:

Professor Pamela A. Abshire, Chair
Professor Ralph Etienne-Cummings
Professor Timothy Horiuchi
Professor Elisabeth Smela

"To the best parents in the world; mine"

ACKNOWLEDGEMENTS

I would like to thank my advisor and mentor Dr. Pamela Abshire for her intellectual support, patient guidance and mentorship. Her vision and constant encouragement were the biggest motivating factors for this work. I thank Dr.Ralph Etienne-Cummings, Dr. Timothy Horiuchi and Dr. Elisabeth Smela for serving on my committee.

I would like to thank my colleagues at the IBIS Lab for a healthy and supportive research environment. I particularly wish to thank Makesh Loganathan for working with me closely on numerous projects. Special thanks to Somasekhar Bangalore Prakash for numerous discussions ranging from technical glitches to food fads. I would like to thank Honghao Ji who had an answer for every technical problem I ever asked him. My thanks to Jean- Marie Launstein, Natasha Reeves, Jack Chaiyupatumpa for working with me on cell recording experiments.

My heartfelt thanks to my friend Sachin Arora for his emotional and intellectual support and patient companionship. I wish to thank Mainak Sen for his optimism and belief in me and for his constant encouragement through times good and bad. My thanks to my friend and room mate Prabha Ramachandran for being the cheerful face at home and making me see the good in all situations.

I wish to thank my family for their love, support and encouragement and taking pride in me and my work. My Dad for being my role model and always teaching me lessons of life in his own special way. My Mom; my pillar of strength for enduring numerous hardships to get me where I am today. My brother for always pushing me in my academic pursuits and the numerous pep talks. My grandparents for their love and blessings.

TABLE OF CONTENTS

LIST OF FIGURES

Chapter 1
Introduction

"No amount of experimentation can ever prove me right; a single experiment can prove me wrong." - Albert Einstein

I present this work as an ongoing effort towards making sensor networks more efficient within the limited resources they have at their disposable. Tradeoffs of performance versus resources are everywhere, placing fundamental and practical limits on performance and efficiency. Highly efficient integrated systems that use minimal energy for maximum impact are essential for autonomous systems whose resources are precious. Transmitting signals is hideously inefficient in light of the inevitable power and bandwidth limitations in sensor networks. Judicious allocation of the resources to maximize the performance of these systems is the key to functional remote and distributed sensing applications. With the growing density of sensor networks, there is a need for systems that operate at low power, have low noise and are efficient in terms of information transfer. Several authors [6,12,21] have investigated the implications of information theory in designing microsystems. Abshire [2] performed an analysis of the information processing in the blowfly photoreceptor and applied the same principles to

studying the information efficiency of silicon photoreceptors. We use principles of information theory and analog circuit design to investigate the performance cost tradeoffs in an Operational Transconductance Amplifier (OTA), a commonly used block in amplification stages in sensory systems.

There is a whole community of designers working on making low voltage, low noise amplifiers for extra-cellular recordings. Harrison [9] designed a low power low noise amplifier for neural recordings applications. Horiuchi et al [10] designed a spike detector for recording from the blowfly photoreceptor. These systems have to be reasonably small, provide good amplification, have frequency selectivity, work at low voltages and have low noise. These requirements become more stringent considering that these circuits are commonly placed in dense arrays and need to be battery powered. We are greedy. We want systems that give us maximum information at minimum cost. In other words, we care about increasing the capacity of these systems for a fixed power budget. We perform detailed analysis to determine how we can maximize the information transfer rate of the OTA.

Chapter2: This chapter is a progress report of our experiments with recording the electrical activity of mammalian cells extra-cellularly. Our current set-up consists of discrete components but we intend to use our custom OTA amplifier in the future. The results of these endeavors give us insight into the spectral and power content of the signals we are trying to measure with our amplifier. This sets the signal power budget and the frequency cut offs for the OTA.

Chapter 3: The block that we choose to optimize in this large sensing scenario is the Operational Transconductance Amplifier. We provide a detailed functional and behavioral analysis of this class A amplifier. The parameters used to characterize the performance of the system are: Open Loop Gain (A_{OL}), Gain Bandwidth Product (GB), Maximum Output Current (I_{OUT}^{MAX}), Slew Rate (SR), Static Power Dissipation (P_{STATIC}), Gain/Phase Margin (GM/PM), Offset Voltage (V_{OS}), Total Harmonic Distortion (THD), Noise (V_{ni}). We are particularly interested in the noise analysis as this is the starting point for doing the information transfer analysis on the OTA structure. We present a detailed description of the noise sources present in a MOS device and their distribution with frequency. The input referred noise for the OTA is determined both for the low frequency and the high frequency case.

Chapter 4: This is the core of our research towards maximizing the capacity of the OTA. We use conventional small signal analysis to determine the transfer functions and input referred noise for the OTA. We model this noise as a colored Gaussian channel with a power constraint and apply the water-filling algorithm to determine the optimal region where we should operate this circuit to achieve maximum capacity. The idea is that since noise is cup-shaped, if we start filling in signal in the region where the noise is minimum then we achieve a high signal-to-noise ratio and hence higher capacity. This happens at considerably higher frequencies. We observe that if we shift the signal to the higher spectral regions, we increase the capacity. We present results from this analytical model corroborating this approach. We have a custom amplifier fabricated in a commercially available 0.5 μm technology. We perform noise and transfer function

measurements on this amplifier and apply the water filling model on the data we collect from these measurements.

Chapter 5: We investigate another criterion for evaluating the efficient performance of our system i.e. capacity per unit cost. We determine how much power is needed to achieve the capacity our circuit can give us. Our definition of power is two-fold: power constraint on the input signal, and supply requirements for the system to operate.

Chapter 6: Noise Efficiency Factor (NEF) is a metric for comparing the noise performance of amplifiers. Since the capacity is a function of the noise performance of the circuit, it is only natural that we extend our model to include the NEF. We determine the capacity of a simple ideal bipolar transistor considering only thermal noise which is the definition for NEF. We compare the capacity of our system with that of a bipolar transistor given similar power constraints and current levels.

Chapter 7: Work to be done: we notice that capacity is maximum if we operate the amplifier at much higher frequencies. But these amplifiers are designed for applications at low frequency. Is it feasible to shift the spectral content of the signal to these higher frequencies without spending more energy in the process? Is it possible to shift the bandwidth of the system to a higher frequency to maximize capacity but keep the desired frequency selectivity of the system? These are some of the issues that will be dealt with in the future.

Chapter 2

Extra-Cellular Recordings from Muscle Cells

Electric current flow in the conductive extra-cellular medium around neurons during action potentials can be detected by means of extra-cellular microelectrodes as voltage 'spikes'. Extra-cellular spike potentials recorded from the mammalian cells have a duration of between 0.2 and 20 millisecond. Their amplitudes are typically a few hundred micro- volts although they may vary in amplitude from the noise level of the electrode (several microvolts) up to several millivolts, depending on the type of cell and the quality of the recording system. The greatest advantage of extra cellular recording is that the activity of cells can be recorded without having to impale and consequently damage them. Most *in vivo* monitoring of electrical properties of the cells is done with extra-cellular recording [25, 26].

Signals picked up by extra cellular electrodes are in the microvolt range and they need to be amplified to be processed in more conventional electronic devices such as oscilloscopes, analyzers or computers. The main difficulty with extra cellular recording is the electrical "noise". This term refers to spontaneous voltage fluctuations, which appear as a thickening of the baseline when viewed on an oscilloscope at low sweep speed. The

noise may result from external interference from electrical sources in the vicinity of the recording set-up (mains line hum pickup) and/or from the intrinsic properties of the substances making up the electrode and electrical circuit (thermal noise) used to amplify electrode signals. Noise in the input circuit and the external medium sets a limit to the minimum amplitude signal that can be reliably measured.

2.1 Electrical Activity is Action Potentials of the Cells

The action potential is a large depolarization signal [14]. It can reach up to 110 mV in amplitude; it lasts only 1 millisecond and can be conducted at rates of 1 to 100 m/s. A sample is shown in Fig 2.1. The action potential is a stereotyped all or none signal. Its amplitude and duration does not depend on the amplitude and duration of the input signal (the synaptic or the receptor potential). Once the firing threshold has been reached the action potential is initiated. Unlike input potentials, which spread passively and decrease in amplitude with distance, the action potential does not decay as it travels along the axon to the terminal of the neuron (this distance can be up to 1meter) [14].

Since the action potential is an all or none signal, a single action potential can not carry information about the amplitude of the input signal. The information of the input potential amplitude is not lost. The integrative component of the cell transforms the amplitude of the input signal into the frequency of an action potential train. In turn, the duration of the input signal is determined by the period during which action potentials are generated.

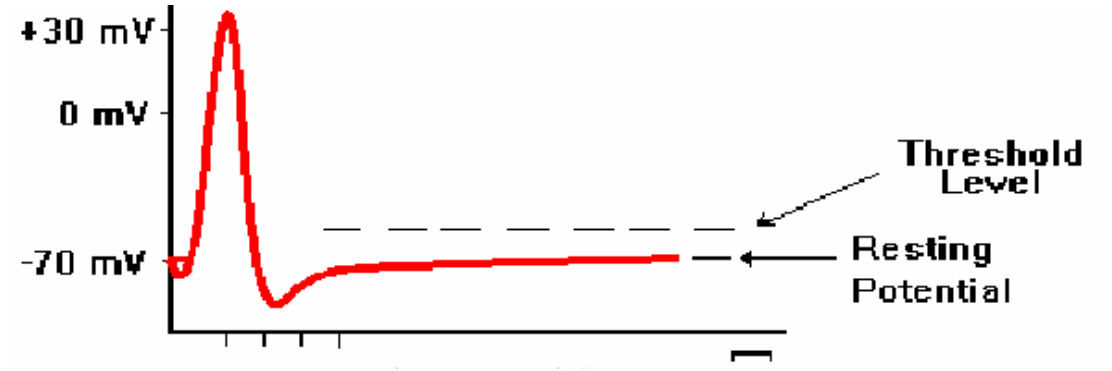

Fig. 2.1 Typical action potential in a neuron [14]

2.2 Experimental Setup for Recording from Cells

Utilizing traditional photolithographic processes to produce planar arrays of microelectrodes has proven to be of immense value to the neuroscience community. There are numerous reports describing the plating of various cell types on planar microelectrode arrays including neurons and cardiac muscle cells [25, 26]. Cardiac cells in culture under proper media and environmental conditions exhibit spontaneous and synchronous action potential activity throughout the culture. By analyzing the signals generated by the spontaneous culture using a microelectrode array, Whittington *et al* [25] were able to monitor the continuous electrophysiological state of the culture and its variation in space and time.

We [20] perform a first run of recordings from Bovine Aortic Smooth Muscle Cells (BAOSMC), which are easy to culture and are known to have electrical activity. Our test set-up shown in Fig 2.2 had the necessary amplification and filtering blocks. A silicon substrate patterned with rectangular gold pads (die) is used as the microelectrode array for the extra-cellular recordings. The conventional aluminum pads are plated with gold since gold is a bio-compatible substance and is mostly non-reactive and non-

corrosive [8]. The cells are left over-night to let them adhere to the pads. Healthy cells spread out, elongate and attach to the pads as shown in Fig 2.3. We [20] examine the test die under the microscope to determine the number of cells adhering to each pad.

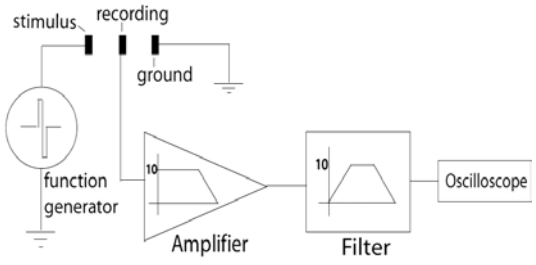

Fig. 2.2 Block diagram of set up for extra-cellular recordings [20]

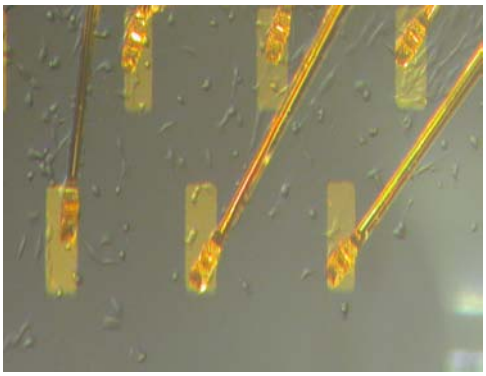

Fig. 2.3 Cells adhered to a silicon substrate

The signals received from the cells are very small in magnitude (μV range), so small that surrounding noise can frequently obscure these signals. Also, these signals are confined to a small bandwidth. We need a set up to filter out the environmental noise (~ 60 Hz) and the noise above the frequencies of interest (above 7 KHz). Since the signal amplitudes lie in micro/milli volts, we need an amplification stage to boost the signal. In order to minimize external noise pickup and interference, experimental set-up has to be correctly shielded and grounded. Overall shielding from noise was provided by placing

test fixture in a die cast aluminum box with a closeable lid. The wire from the electrode to the output was kept as short as possible, less then 2" (5 cm). Line-powered equipment was kept as far away from the site of recording as possible. Everything near the preparation is grounded to a single point.

The test die is packaged in a DIP package and a vector board as shown in Fig. 2.4 was made for the measurements.

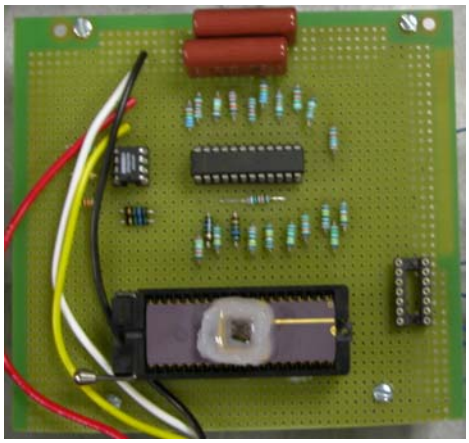

Fig. 2.4 Passive fixture for recording from the cells

A thick well of conductive epoxy was put around the die to isolate the packaging material from the cells and also to protect the bond wires. The components on the board include an amplifier and a band pass filter. The amplifier receives the signal from the cells and magnifies it 10 times. This amplification is applicable to the noise associated with the signal as well. This amplified signal is then given to a band pass filter, since we want to remove the low frequency 60 Hz noise and the high frequency (above 7 KHz) noise. The band pass filter can also be used to amplify the filtered signal by a factor of 10. The amplifier we used is a high precision low noise amplifier OPA227. The amplifier was

tuned to give a gain of 10.The filter we used is the Maxim 274 continuous time active filter consisting of four independent cascadable second order sections. We designed each of these sections to be Butter Worth band pass filters centered at 1.5 kHz and having a pass band between 500 Hz and 5 kHz with a midband gain of 10. The recorded output is 100 times amplified.

2.3 Cell Recordings

To get an estimate of the noise associated with the set up and the growth medium, we recorded from the growth medium and de-ionised water before recording from the cells. Shown in Fig 2.5 is a sample of our recordings where the noise shown (between the blue lines) is an average of our recordings without cells.

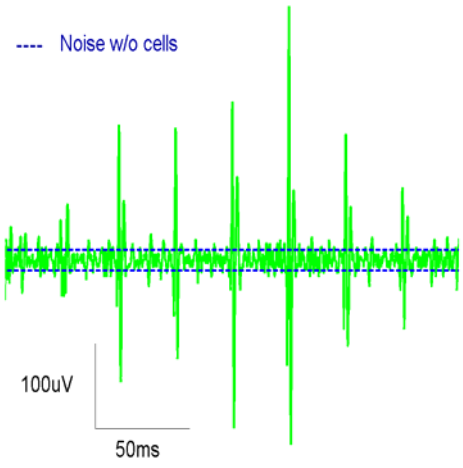

Fig. 2.5 Sample of recordings from the cells

2.4 Conclusion

We [20] perform the extra-cellular measurements of the stimulated and spontaneous action potentials of the mammalian cells. We accomplish two objectives: we prove the

electrically activity of the BAOSMC and also determine amplitudes and bandwidth of the action potentials of these cells. This gives useful information about the amplification and filtering limits for the amplifier design.

Currently, as shown our [20] set-up is made up of discrete components. The next stage of recordings will be done with cells placed on the custom OTA amplifier.

Chapter 3

Operational Transconductance Amplifier (OTA)

In order to optimize a system it is imperative to analyze it completely. We present a detailed description of the structure of OTA and the various characterization parameters. This is the first step towards formulating the model for information capacity for a particular system. The schematic symbol and equivalent circuit model for an Operational Transconductance Amplifier (OTA) are shown in Fig 3.1 [7,13,19].

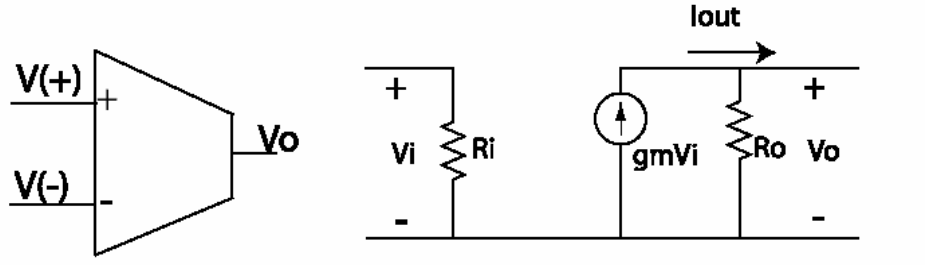

Fig. 3.1 OTA Symbol and Equivalent Circuit

The OTA converts a differential input voltage to an output current relative to a transconductance gain parameter $Gm=i_o/v_i$. Ideally, the input and output resistances are infinite ($R_i = R_o = \infty$) such that $i_i = i_{Ro} = 0$ and the output current is absorbed solely by the load. The conventional OTA is classified as a class A amplifier and is capable of generating maximum output currents equal to the bias current applied. The equivalent circuit model indicates that the transconductance amplifier generates an output current

(i_o) proportional to an input voltage (v_i) based on the transconductance gain G_m. The open circuit voltage gain of the conventional OTA model in Fig 3.3 is given by $A=G_m R_o$.

A conventional, one stage, CMOS, Operational Transconductance Amplifier (OTA) configuration is shown in Fig 3.2

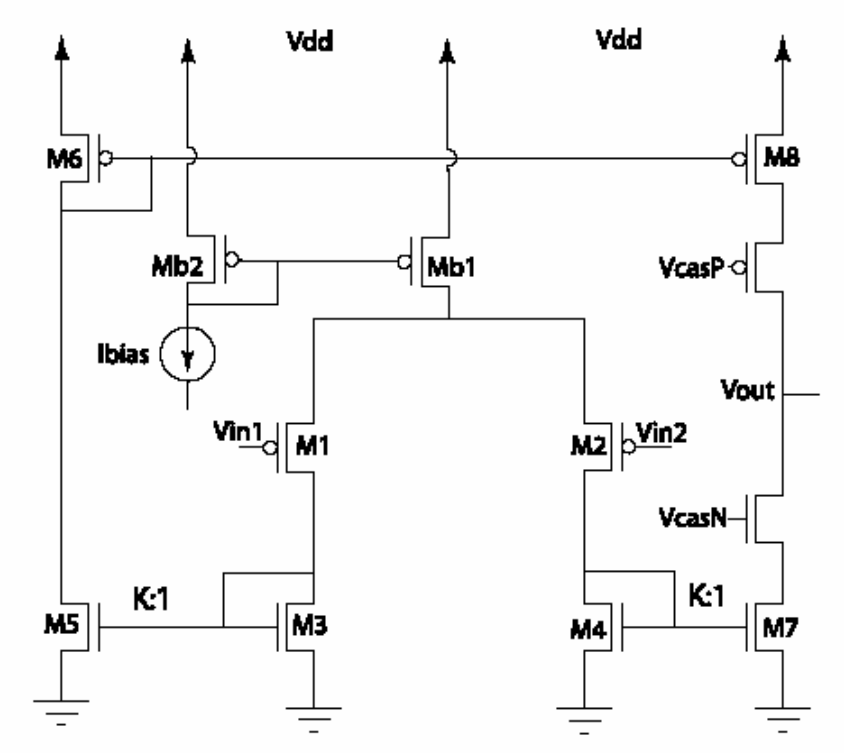

Fig. 3.2 A single stage Operational Transconductance Amplifier

The OTA employs a differential input pair and three current mirrors. The differential input pair is comprised of transistors $M_{1,2}$. The differential pair is biased by $M_{B1,B2}$. Mirrors formed by $M_{3,5}$ and $M_{4,7}$ reflect currents generated in the differential pair to the output shell. The current generated by the mirror of $M_{3,5}$ is then reflected to the output via the mirror formed by $M_{6,8}$. The mirror gain factor, K, indicates the gain in mirrors formed by $M_{3,5}$ and $M_{4.7}$. Cascoding transistors $M_{casN,casP}$ are biased by V_{casN} and V_{casP} respectively and provide increased gain via increased (cascoded) output resistance.

The conventional OTA is differentiated from other amplifiers by the fact that its only high impedance node is located at the output terminal. The OTA [13] does not employ an output buffer and is therefore, only capable of driving capacitive loads.

3.1 Operation

The conventional OTA uses a differential pair in conjunction with three current mirrors to convert an input voltage into an output current. Common mode signals ($V_{in1}=V_{in2}$) are, ideally, rejected. For a common mode input voltage, the currents are constant and will be: $i_{d1}=i_{d2}=I_{BIAS}/2$ and $i_{out}=0$. A differential input signal will generate an output current proportional to the applied differential voltage based on the transconductance of the differential pair. The conventional OTA is only capable of producing an output current with a maximum amplitude equal to the bias current in the output shell. For this reason, the conventional OTA is a referenced as a class A structure capable of producing maximum signal currents equal to that of the bias current applied. Slew rate (SR) is directly proportional to the maximum output current and is defined as the maximum rate of change of the output voltage. For a single stage amplifier, the slew rate is the output current divided by the total load capacitance. The conventional OTA therefore suffers the consequence that high speed requires large bias currents which translates to large static power dissipation.

3.2 Small Signal Analysis

We perform a detailed small signal analysis for determining the transfer function, the bandwidth and noise transfer functions for the OTA information capacity model.

3.2.1 Open loop gain

Fig 3.3 will be used for the open loop gain analysis. The output current, in terms of the mirror gain factor (K), is given by:

$$i_{out} = Ki_{d2} - Ki_{d1} \tag{1}$$

where:

$$i_{d1} = g_{m1}V_{in1}, i_{d2} = g_{m2}V_{in2} \tag{2}$$

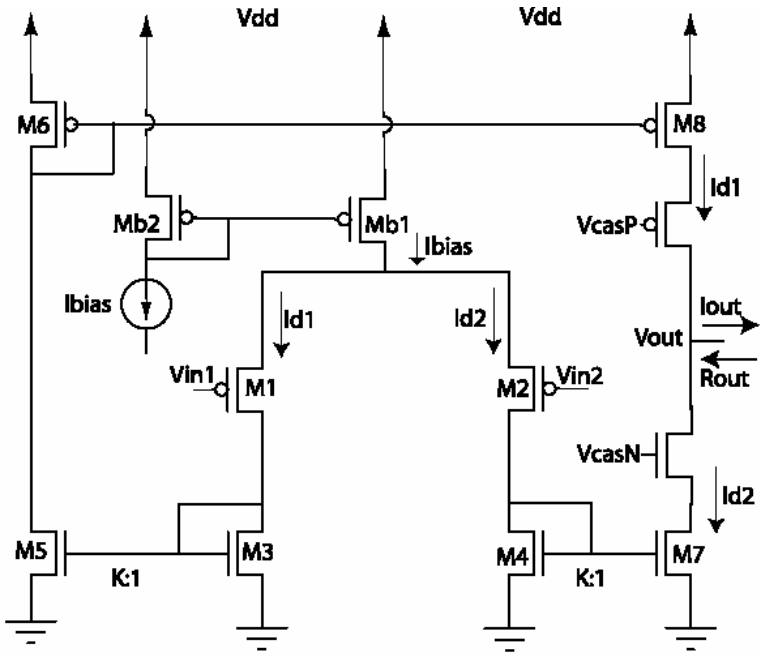

Fig. 3.3 OTA open loop gain schematic

Assuming: $g_{m1}=g_{m2}$, and substituting (2) in (1)

$$i_{out} = Kg_{m1,2}(V_{in1} - V_{in2}) \tag{3}$$

This indicates the transconductance gain of the OTA is given by:

$$G_m = Kg_{m1,2} \tag{4}$$

The output resistance is a cascode resistance and is given by:

$$R_{out} = g_{mN}r_{oN}r_{o7} \parallel g_{mP}r_{oP}r_{o8} \tag{5}$$

Combining (3) and (5), the output voltage is then given by:

$$v_{out} = i_{out} R_{out} = K g_{m1,2} (V_{in1} - V_{in2})(g_{mN} r_{oN} r_{o7} \| g_{mP} r_{oP} r_{o8}) \tag{6}$$

and the open loop gain is:

$$A_{OL} = \frac{v_{out}}{v_{in}} = K g_{m1,2} (g_{mN} r_{oN} r_{o7} \| g_{mP} r_{oP} r_{o8}) \tag{7}$$

3.2.2 AC Analysis

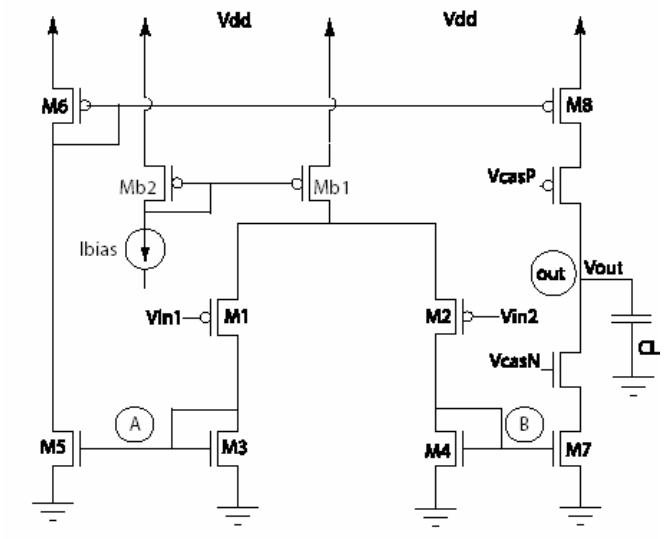

Fig. 3.4 OTA AC Analysis schematic

The gain bandwidth of the single stage OTA is limited mainly by the low impedance, high frequency poles at nodes A and B, in conjunction with the high impedance, low frequency pole at the output node. The following analysis will define the high frequency pole and will assume nodes A and B are equivalent nodes in terms of resistance and parasitic capacitance (M_1=M_2, M_3=M_4= M_5=M_6). The resistance at nodes A and B is dominated by the diode connected resistance ($1/g_m$) of $M_{3,\,4}$ and is given by:

$$R_{A,B} = \frac{1}{g_{m3,4}} \left\| r_{01,2} \approx \frac{1}{g_{m3,4}} \right. \tag{8}$$

The parasitic capacitance at A and B is given by:

$$C_{A,B} = C_{gd1,2} + C_{gs3,4} + C_{gs5,7} + C_{gd5,7} \approx C_{gs3,4} + C_{gs5,7} \tag{9}$$

The pole at A and B is

$$f_{pA,B} = \frac{1}{2\pi C_{A,B} R_{A,B}} = \frac{g_{m3,4}}{2\pi(2C_{gs3,4})} \tag{10}$$

The output node capacitance is dominated by the load capacitance (C_L) and is:

$$C_{out} = C_{gdN} + C_{gdP} + C_L \approx C_L \tag{11}$$

Combining (10) and (11), the dominant pole/bandwidth of the OTA is given by:

$$f_{pout} = \frac{1}{2\pi C_{out} R_{out}} = \frac{1}{2\pi C_L (g_{mN} r_{oN} r_{o7} \,||\, g_{mP} r_{oP} r_{o8})} = f_{3dB} \tag{12}$$

Equation (10) indicates the high frequency pole $f_{PA,B}$ is inversely proportional to $C_{gs3,4}$. The bandwidth of the conventional OTA is given in Equation (12) and is inversely proportional to the load capacitance (C_L).

3.2.3 Gain Bandwidth

Equations (7) and (12) are combined for the gain bandwidth (GB) product:

$$GB = \frac{Kg_{m1,2}}{2\pi C_L} \tag{13}$$

This relation indicates that the GB is directly proportional to the mirror gain factor K.

3.2.4 Maximum Output Current

The maximum output current of the conventional OTA is limited by the bias current and is given by:

$$I_{out}^{MAX} = KI_{BIAS} \tag{14}$$

3.2.5 Slew Rate

The slew rate is given by

$$SR = \frac{I_{out}^{MAX}}{C_L} = \frac{KI_{BIAS}}{C_L} \tag{15}$$

The slew rate increases linearly with I_{BIAS} and the current mirror gain factor K.

3.3 DC Analysis

3.3.1 Input Common Mode Range

The common mode range (CMR) is defined as the range of voltage (V_{IN}^{MIN}, V_{IN}^{MAX}) for which the input differential pair will remain in saturation. This range is determined by the amplifier structure, transistor sizes, and bias current. For the differential input stage with diode connected loads, the minimum and maximum input voltages can be found by analysis of Fig 3.5.

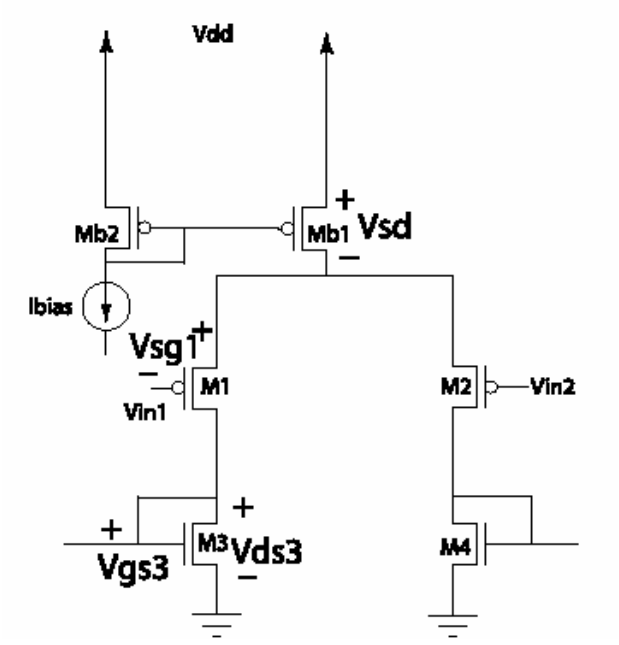

Fig. 3.5 Input differential pair with diode connected load

3.3.1.1 Minimum Input Voltage

The minimum input voltage can be expressed as:

$$V_{IN}^{MIN} = V_{DD} - (V_{DSMB1} + V_{DS1}^{SAT} + V_{THP1}) \tag{16}$$

and substituting:

$$V_{DS}^{SAT} = \sqrt{\frac{2I_D L}{WKP}} \tag{17}$$

The minimum input voltage becomes:

$$V_{IN}^{MIN} = V_{DD} + \sqrt{\frac{2I_{BIAS}L_{MB1}}{W_{MB2}KP_P}} + \sqrt{\frac{I_{BIAS}L_1}{W_1 KP_P}} + V_{THP1} \tag{18}$$

where V_{THP1} is body effected and may be larger than the zero bias threshold voltage. The minimum input voltage is therefore limited by the $V_{DS,\,SAT}$ drop requirements across M_1, M_{B1} and a threshold drop across M_1. The minimum input voltage is inversely proportional to the widths of transistors M_1, M_{B1} and directly proportional to the bias current. To reduce V_{IN}^{MIN}, bias current must be reduced or the widths of the input transistors must be increased.

3.3.1.2 Maximum Input Voltage Range

The maximum input voltage can be expressed:

$$V_{IN}^{MAX} = V_{SS} + V_{GS3} + V_{THP1} \tag{19}$$

and with substituting V_{GS3}, it becomes

$$V_{IN}^{MAX} = V_{SS} + \left[\sqrt{\frac{I_{BIAS}L_3}{W_3 KP_N}} + V_{THN3}\right] + V_{THP1} \tag{20}$$

Again, V_{THP1} is body effected and will be larger than anticipated. In this case, the body effect actually increases input range by contributing to V_{IN}^{MAX}. These results indicate the bias current must be reduced and the width of M_3 must be increased to increase V_{IN}^{MAX}.

The maximum input voltage is, therefore, only limited by a V_{GS} drop across M_3. For this reason, the input voltage range is typically limited by V_{IN}^{MIN}. The common mode range of the PMOS differential pair is capable of swinging further in the negative direction than the positive direction.

3.3.2 Output Voltage Range

The output voltage range is defined as (V_{OUT}^{MAX}, V_{OUT}^{MIN}) which represents the maximum output swing available. The output range of the conventional OTA is reduced due to cascoding at the output shown in Fig 3.6

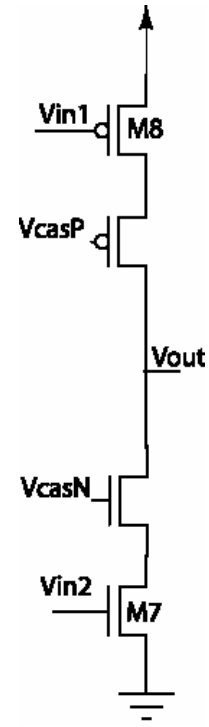

Fig. 3.6 OTA cascoded output

The output voltage range is given as:

$$V_{out}^{MAX} = V_{DD} - V_{DS,SAT8} - V_{DS,SATP} \tag{21}$$

$$V_{out}^{MIN} = V_{SS} + V_{DS,SAT7} + V_{DS,SATN} \tag{22}$$

3.3.3 Static Power Dissipation

The static power dissipation (P_{STATIC}) is the product of the sum of the currents flowing through the current sources or sinks with the power supply voltages and is given by:

$$P_{STATIC} = (V_{DD} - V_{SS})[I_{D,MB1} + I_{D,M1} + I_{D,M2} + I_{D,M5} + I_{D,M7}] \quad (23)$$

and in terms of I_{BIAS}

$$P_{STATIC} = (V_{DD} - V_{SS})I_{BIAS}(2 + K) \quad (24)$$

An increase in the I_{BIAS} will increase the SR and GB of the conventional OTA at the cost of increased area and static power dissipation and a decrease in phase margin.

3.4 Characterization

3.4.1 Gain and Phase Margins

The application of negative feedback requires analysis of the open loop gain. Some circuits will cause a phase shift in the input signal large enough that the feedback becomes positive (adds to the input), resulting in an unstable system [7]. Stability requires a phase shift in the feedback signal less than 180° for open loop gain values larger than 0 dB. This requirement necessitates the definition of two measures of stability: gain margin (GM) and phase margin (PM). Gain and phase margin parameters can be measured via analysis of the open loop AC response simulation. The gain margin is defined as the difference (in dB) in the gain at a phase of -180° and unity gain. Design guidelines typically specify a GM greater than 10 dB. The phase margin is defined as the difference (in degrees) in the phase at unity gain and -180°. The phase margin should be

greater than 45° with an optimum, critically damped, value of 60° [3]. For PM values less than 60° the system is under-damped, and the transient response will indicate increased slew rate. For PM values greater than 60° the system is over-damped, and the transient response will indicate decreased slew rate. Phase margin depends on the relative position of the high frequency pole f_{PA} (Fig 3.4) and the gain bandwidth (unity gain frequency). The position of the high frequency pole location is therefore directly related to the phase margin.

3.4.2 Input Offset Voltage

Ideally, if both inputs of the OTA are grounded, the output voltage should be zero [7]. Practically, a nonzero output voltage (offset) will be present and is due to random and systematic errors.

3.4.2.1. Random Offset

Random errors are due to mismatches in the input stage as a result of fabrication including (but not limited to) : threshold voltage differences and geometric differences. Random errors can be estimated via Monte Carlo simulations.

3.4.2.2 Systematic Offset

Systematic errors are inherent to the design. Systematic errors can be the result of non-symmetries in the OTA design, creating voltage and current mismatches. The systematic offset can be determined via simulation and will be evident in the DC sweep simulation as the offset from the zero-zero intercept where the input voltage and output voltage should both equal zero.

3.4.3 Total Harmonic Distortion

Ideally, the output of an amplifier is a replica of the input signal scaled by the gain A.

The gain for large signal inputs is dependent on the input signal amplitude [7]. For a purely sinusoidal input signal:

$$V_{in}(t) = V_M \sin(wt) \tag{25}$$

The non-ideal output signal of an amplifier can be expressed as:

$$V_{OUT}(t) = a_1 V_M \sin(\omega t) + a_2 V_M \sin(2\omega t) + ... + a_n V_M \sin(n\omega t) \tag{26}$$

where the desired output is a fundamental $a_1 V_M \sin(\omega t)$ and ideally a_2 through a_n are zero.

3.4.4 Noise sources in OTA

Analog signals, processed by integrated circuits, are corrupted by two different types of noise: device electronic noise and "environmental noise". Noise limits the minimum signal level that a circuit can process with acceptable quality. Today's analog designers constantly deal with the problem of noise because it trades with power dissipation, speed and linearity. Doing efficient design requires that noise be taken into account as readily as any other circuit parameter like gain, input, output impedance etc.

Next we discuss the noise sources in a MOSFET and consider methods of representing noise in circuits [19].

3.4.4.1 MOSFET Thermal noise

The most significant source [17] is the noise generated in the channel. The random thermal motion of electrons in the channel introduces fluctuations in the voltage measured across the channel even if the average current is zero. Thus the spectrum of the thermal noise is proportional to absolute temperature T. The dependence of thermal noise upon temperature suggests that low temperature operation can decrease the noise in analog circuits. The thermal noise can be modeled by a current source connected between the drain and source terminals as shown in Fig. 3.7 with spectral density given by [19]

$$\overline{I_n^2} = 4kT\gamma g_m \tag{27}$$

where k is the Boltzmanns constant , T is the absolute temperature in Kelvin, g_m is the device transconductance.γ is a constant [5] taken to be 2/3 for above threshold and 1/2 for below threshold conduction for long channel transistors. Their values for short channel transistors is still a topic of research.

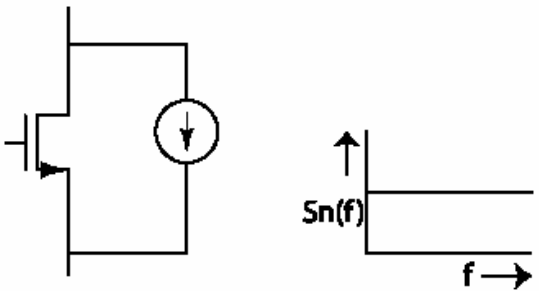

Fig. 3.7 MOSFET noise current source model for thermal noise

3.4.4.2 Flicker noise

Flicker noise is present under DC conditions and is the result of electron trapping (delayed release) due to silicon imperfections in the transistor. Flicker noise is inversely proportional to frequency and is commonly referred to as 1/f noise. The flicker noise can be modeled with a current source with spectral density [3] in parallel with the transistor as shown in Fig 3.8

$$\overline{I_{n,1/f}^2} = \frac{KF * I_D^{AF}}{C_{ox}(g_m^2)f} \tag{28}$$

KF is a process-dependent flicker noise constant with approximate value of 10^{-25} V^2 F.

AF is a constant with its value lying between 0.5 and 2, I_D is the drain current (DC), C_{ox} is the capacitance per unit area, g_m is the device transconductance and f is the frequency.

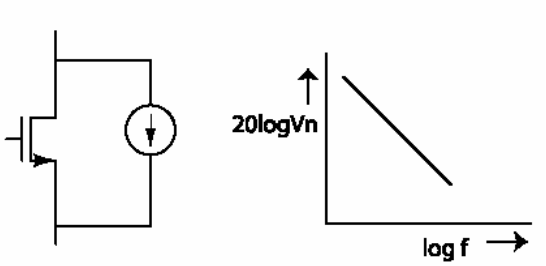

Fig. 3.8 MOSFET noise current model for flicker noise

The noise sources are given in terms of per unit bandwidth. There can be an interesting possibility of lower frequency cut-off flicker noise being zero [19]. As the flicker noise has a logarithmic dependence on frequency this yields an infinite value for total noise. Secondly if we observe the circuit for a very long time, the very slow noise components can randomly assume a very large power level. At such slow rates, noise becomes indistinguishable from thermal drift or aging of devices. This leads to the following conclusions: first since the signals encountered in most applications do not contain significant low frequency components, our observation window need not be very long. Secondly, the logarithmic dependence of flicker noise over f_l allows some margin of error in selecting f_l.

To quantify the significance of 1/f noise with respect to thermal noise for a given device, we plot both spectral densities on the same axes and determine their intersection point. Called the "corner frequency", the intersection point serves as a measure of what part of the band is mostly corrupted by flicker noise.

$$f_c = \frac{K}{C_{ox} WL} g_m \frac{3}{8kT} \tag{29}$$

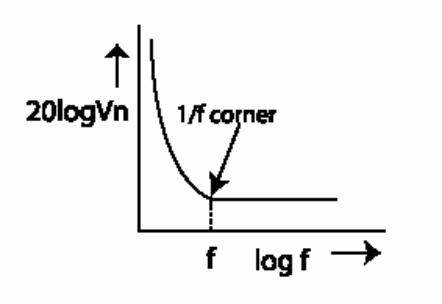

Fig. 3.9 Total noise spectrum

3.4.4.3 Representation of noise in circuits

The natural approach to quantify the effect of noise in a circuit is to calculate the total noise at the output due to the various sources of noise in the circuit. While intuitively appealing, the output-referred noise does not provide a useful comparison of the performance of different circuits because it depends on the gain.

Consider a system with noise at the output [19] equal to V_{nout}^2 followed by an amplifier at the output stage of gain A2 as shown in Fig 3.10. Then the total output noise is equal to the V_{nout}^2 multiplied by A2. Considering only the output noise we may conclude that if the gain A2 increases, the circuit becomes noisier which is an incorrect result because a larger A2 also provides a proportionally higher signal level at the output. That is the output signal to noise ratio does not depend on A2.

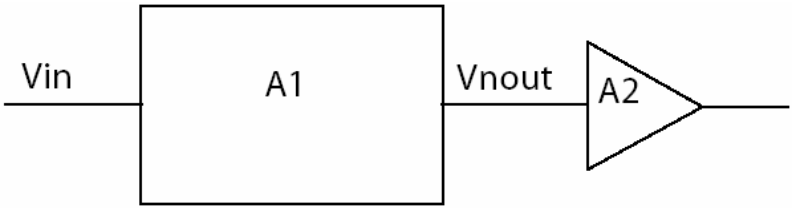

Fig 3.10 Additional gain stage at the output

To overcome this quandary we specify the "input-referred noise" of the circuits [17]. The idea is to represent the effect of noise sources in the circuit by a single source $V_{n,in}^2$ at the input such that the noise at the output is equal to the output noise if all the noise sources

in the circuit were to be considered separately. If the voltage gain is A_v, then we must have $V_{n,out} = AV_{n,in}^2$, i.e the input referred noise in the simple case is the output noise voltage divided by the gain.

3.5 Conclusions

A full analysis of the one-stage conventional OTA structure was presented to determine the transfer functions and noise contributions of each device in the OTA to the total noise at the output. This is the basis for the model for information capacity. The transconductance amplifier rejects common mode signals and generates an output current dependent on the input voltage. Cascoding of the output shell to increase gain necessitates the requirement of a purely capacitive load. The structure is class A and the maximum output current is limited by the magnitude of the bias current in the output shell. The mirror gain factor K can be increased to increase the maximum output current (slew rate) and gain bandwidth at the cost of an increase in static power, and area, as well as a decrease in phase margin and stability.

This OTA forms the core of our custom amplifier for recording the electrical activity of mammalian cells. It is to be optimized to give a good gain and frequency roll off at high frequencies. We treat the OTA as a Gaussian channel with a power constraint and determine the optimal region of operation of the circuit for maximum information transfer rate. In the subsequent chapters we develop this approach and use different metrics for evaluating the performance of the OTA.

Chapter 4

Information Capacity in OTA

The transmission of data through analog systems is corrupted by the intrinsic thermal and flicker noise in these systems. The degradation can be significant when signal power and noise power are comparable. Noise in the input can lead to a considerable loss of information while noise at the output is less prohibitive once signal power has been boosted by amplification. Special care must be given to reduce noise at the input stage, particularly for low power signals.

In many applications, the frequency range of operation of the analog system is specified by the spectral power content of the input signal, determined by the environment and input statistics for particular applications. Examples of such systems are an amplifier recording signals from electrically active cells and an imager acquiring images from natural scenes. The power of these signals is concentrated at low temporal frequencies. However we know from basic noise theory [17] that semiconductor device noise is concentrated at these low frequencies, and hence the design of these sensor systems considerably reduces the signal to noise ratio (SNR) resulting in a reduction in the information content. If we operate these amplifiers at frequencies where their noise level is minimized, then we achieve an increase in SNR and consequently the information content.

4.1 Introduction

To formulate our model, we briefly introduce the relevant concepts from information theory. Consider a general communication system [4, 22] consisting of an input, a channel, a noise source and the output as shown in Fig. 4.1

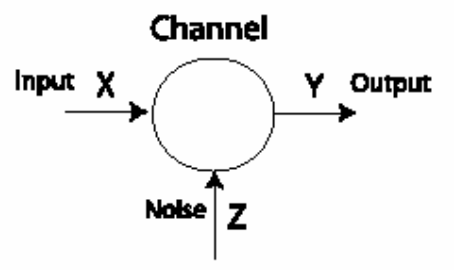

Fig. 4.1 A Gaussian channel [22]

Uncertainty in the system is modeled as an additive noise contribution Z at the output of the channel, such that Y = [X] + [Z] where X and Y are the input and output signals respectively. The information rate through the system is limited by the channel bandwidth F and the noise power N corrupting the signal. The channel capacity is determined by maximizing the mutual information I(X;Y) between the input and the output. We model the system as a Gaussian channel transmitting information at a rate R.

A **Gaussian channel** is an additive noise channel where the noise is a random Gaussian process. For a Gaussian channel [22], the transmission bandwidth and the ratio of the signal power to noise power are sufficient to determine the channel's capacity to transmit information. The noise entropy per second is $H(Z) = F \log_2 \pi eN$, where F is the bandwidth of transmission over the channel and $N = \sigma_z^2$ is the noise power. With no constraints on the input, we are free to choose input levels spaced arbitrarily far apart, and there is little trouble in distinguishing the outputs. The capacity is unbounded. However, unconstrained inputs are physically implausible. We'll resolve this difficulty by imposing a power limitation P on the input signal, so

that $\frac{1}{n}\sum_{i=1}^{n} x_i^2 \leq P$. The Gaussian distribution maximizes the entropy for a fixed variance, so the output entropy per second is bounded by the entropy of a Gaussian distribution with the same output power $H(Y) \leq F \log_2 \pi e(P+N)$. This leads to the famous result given by Shannon for the channel capacity of a Gaussian channel; $C = F * \log_2\left(1+\frac{P}{N}\right)$ where P and N are the average signal and noise power, respectively, and the capacity C is given in units of bits per second. This result applies to channels with an average signal power constraint P and additive white Gaussian noise of power N. The expression of the channel capacity of the Gaussian channel makes intuitive sense:

- As the bandwidth of the channel increases, it is possible to make faster changes in the information signal, thereby increasing the information rate linearly.

- As S/N increases, one can increase the information rate while still preventing errors due to noise.

- For no noise, $S/N = \infty$ and an infinite information rate is possible irrespective of bandwidth.

If a white thermal noise is passed through a filter whose transfer function is Y (f), the resulting noise has a power spectrum N (f) = K $|Y(f)|^2$ and is known as Gaussian noise. We can calculate the capacity of a channel perturbed by any Gaussian noise from the white-noise result. Suppose our total transmitter power is P and it is distributed among the various frequencies according to P (f).

Then, $\int_0^W P(f)df = P$ (1)

We can divide the band into a large number of small bands, with approximately N (f) constant in each. The total capacity for a given distribution P (f) will then be given by

$$C_1 = \int_0^W \log\left(1+\frac{P(f)}{N(f)}\right) df \tag{2}$$

since, for each elementary band, the white-noise result applies. The maximum rate of transmission will be found by maximizing C_1 subject to condition (1). We use Lagranges multipliers [1] to do this.

$$\int_0^W \left[\log\left(1+\frac{P(f)}{N(f)}\right)+\lambda P(f)\right] df \tag{3}$$

The condition for this is, by the calculus of variations, or merely from the convex nature of the curve log (1+x)

$$\frac{1}{N(f)+P(f)}+\lambda = 0 \tag{4}$$

or N (f) + P (f) must be constant. The constant is adjusted to make the total signal power equal to P. For frequencies where the noise power is low, the signal power should be high and vice versa as we would expect.

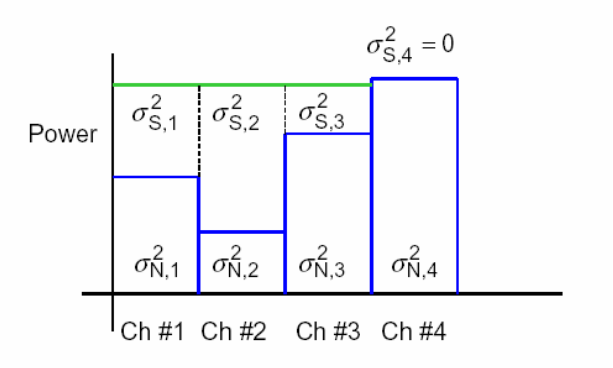

Fig 4.2 Water filling

The signal that maximizes the capacity can be found using the water-filling analogy [4]. Shown if Fig 4.2 is a system with multiple channels each having a different noise distribution. Given the total power P to be distributed among the different channels in the system, water filling tells us to allocate power to the channels which has the lowest noise first and then progressively to the noisier channels. If P is small, we

cannot make P (f) + N (f) constant, since this would require negative power at some frequencies. It is easily shown, however, that in this case the best P (f) is obtained by making P (f) + N (f) constant whenever possible, and making P (f) zero at other frequencies. With low values of P, some of the frequencies will not be used at all. If we now vary the noise spectrum N (f), keeping the total noise power constant and always adjusting the signal spectrum P (f) to give the maximum transmission, we can determine the worst spectrum for the noise. This turns out to be the white-noise case. It is not just the worst among the Gaussian noise sources, but also among all possible noises with the given power in the band.

We wish to maximize the information transfer between the input and output for the OTA. The starting point for that is maximizing the information capacity, since the capacity of a channel depends only on the channel properties and signal constraints, such as bandwidth, noise, and constraints on the signal values; it does not depend on the specific details of any particular task for which the channel may be used [22]. There have been successful efforts in optimizing the performance of analog circuits, considering them as a channel [2,12]. The input referred noise waveform can be calculated from transfer function analysis, and the entire circuit can be modeled as an information transfer channel corrupted by colored Gaussian noise. The efficiency of information transfer through this circuit can be maximized by concentrating signals in spectral regions where the channel noise is minimal. As the input referred noise is typically cup-shaped, the water filling technique provides the most efficient distribution of signals in channels with colored Gaussian noise. Just as water distributes itself in a vessel, the power in a given system is allocated to frequency bands starting from the spectral region with lowest noise and then spilling over to the

noisier parts of the channel [4]. We apply this algorithm to obtain the ideal frequency range of operation of an OTA for maximum information transfer.

4.2. System Topology

We consider a generic system consisting of n analog blocks A1, A2…An with equivalent input noise sources V1, V2 …Vn as shown in Fig. 4.3. The noise from each block is assumed to be composed of a flicker noise source and a white Gaussian noise source [15]. We treat the entire system as a colored Gaussian channel and estimate the ideal frequency range of operation for maximum information transfer rate.

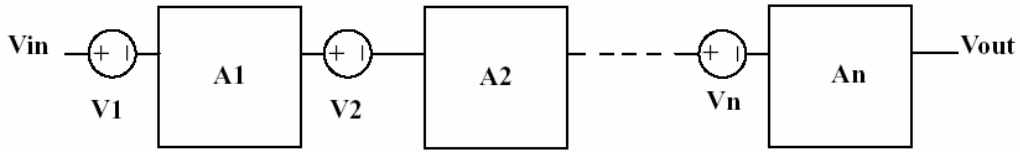

Fig 4.3 System comprising of n blocks A1, A2 … An

4.2.1. Low Frequency Analysis

At low frequencies, the transfer function of each block is perfectly flat. The input referred noise of the system is given by Equation (5) and shown in Fig 4.4 (a). We assume that there is a brick wall filter at the output of the system that blocks all frequencies above frequency Fmax to restrict attention to the low frequency case.

$$\overline{V_{IN}^2} = \overline{V_1^2} + \frac{\overline{V_2^2}}{A_1^2} + \ldots\ldots \frac{\overline{V_n^2}}{A_1^2 A_2^2 \ldots\ldots A_{n-1}^2} \tag{5}$$

We know that the capacity C of a channel or the maximum information transfer rate is given by

$$C = \max_{S(f):\sigma^2<P} \int_{f1}^{f2} \log_2\left(1+\frac{S(f)}{N(f)}\right) df \tag{6}$$

where S (f) and N (f) are signal and noise power spectral densities and the maximization is over all the signals such that the average signal power is less than the power constraint P. The frequency range (f_2-f_1) defines the bandwidth of interest.

To transmit a signal satisfying the average power constraint through this system with maximum efficiency, the water-filling approach tells us that we should start filling at F_{max} and add power at progressively lower frequencies until we reach the total power content in the signal. This result follows from the observation that input referred noise spectral density is a monotonically decreasing function of frequency. The distribution of the signal power for maximum information transfer rate is shown in Fig. 4.4 (b).

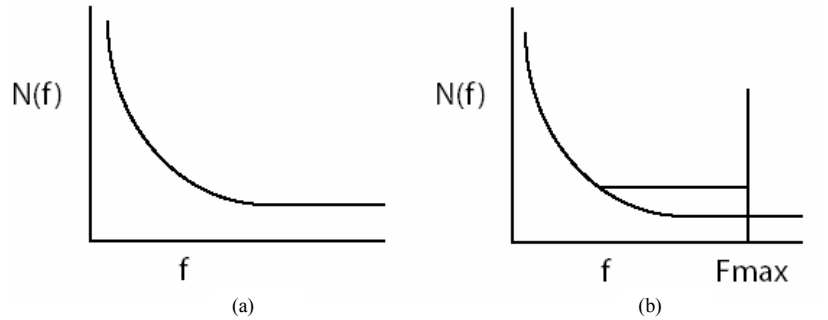

Fig 4.4 (a) Input referred noise of the system, (b) Ideal distribution of Power for maximum information transfer rate.

This differs from the traditional approach of using the systems at low frequencies near the first pole. If we shift the operation of the system to higher frequencies, where noise is reduced, we will achieve an increase in the signal to noise (SNR) ratio and hence capacity of the system.

4.2.2. High Frequency Analysis

Under typical working conditions, the transfer functions of these analog blocks vary with frequency. We consider a cascade of low pass blocks, and the transfer function A1, A2 ... An of each of the blocks are as shown in Fig.4.5 (a). The noise contribution from each block is assumed to be similar to that shown in Fig 4.4(a). The input referred noise of the system is calculated using Equation (5) and plotted in Fig 4.5(b).

For efficient use of this system, we should start filling up the signal from the lowest point in the noise spectrum and continue till we reach the total power content of the signal. This contrasts sharply with the regular usage of the system at frequencies below the most dominant pole (f1). Conventionally the amplifiers are used within their 3 dB bandwidth where they have maximum gain and maximum noise. Fig 4.5(c) shows the system being used at frequencies below f_1, and Fig 4.5(d) shows the most efficient region of operation of the system.

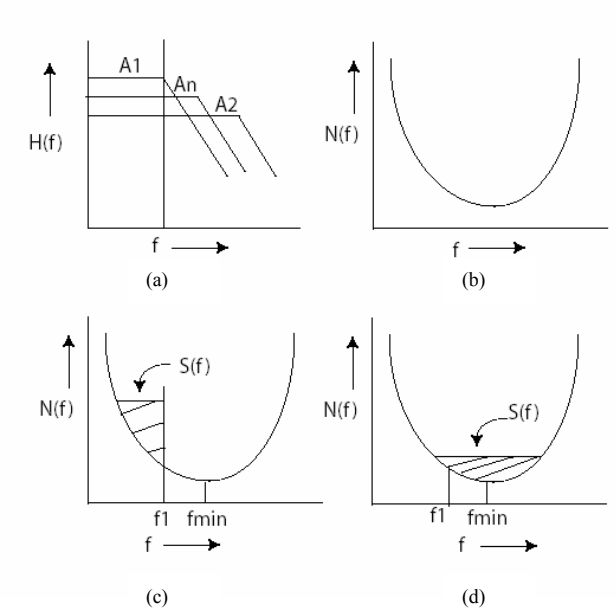

Fig 4.5 (a) Transfer functions of each of the blocks A1, A2… An
(b) Input referred noise of the entire system, (c) Regular use of the system, (d) Ideal distribution of Power for maximum information transfer rate. f1 is the most dominant pole of the system, fmin corresponds to the lowest noise level.

4.2.3 Noise at the Output

The noise of the stage following the system should also be modeled as either a white or a colored Gaussian channel depending on its spectrum. If the noise is an order of magnitude smaller than the system noise, then it will not affect the performance of the system. If they are comparable, the effective input referred noise of the system should include this noise too, and then water filling should be performed on the total input referred noise.

4.2.4 Effect of Feedback on Input Noise

Let us consider a simple first order feedback system as shown in Fig 4.6(a) [19], where the block A1 is an open loop voltage amplifier characterized by only an input referred noise V_n and the feedback network is noiseless. We have

$$(V_{in} - \beta V_{out} + V_n)\, A_1 = V_{out} \tag{7}$$

Hence, $$V_{out} = (V_{in} + V_n)\frac{A_1}{1 + \beta A_1} \tag{8}$$

The circuit can be simplified as shown in Fig 4.6(b) revealing that the input referred noise of the overall circuit remains equal to V_n. If the feedback network were to introduce noise at the output, then the introduction of feedback reduces system capacity and power efficiency.

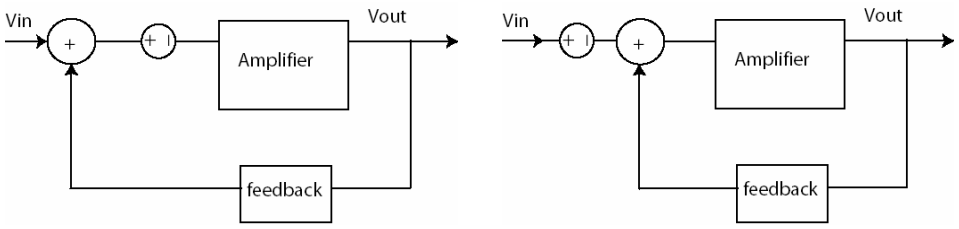

(a) (b)

Fig 4.6 (a) A simple first order feedback system, (b) Equivalent schematic of the system

4.3. Practical Amplifier Configurations

Based on the generic system topology we discuss above, we perform this information capacity analysis on a custom amplifier which is an Operational Transconductance Amplifier in capacitive feedback configuration. Our analysis considers the feedback network consisting of the capacitors to be noiseless.

4.3.1. Operational Transconductance Amplifier

We perform noise analysis on a simple cascoded OTA [9], and then apply the water filling approach to the noise waveform.

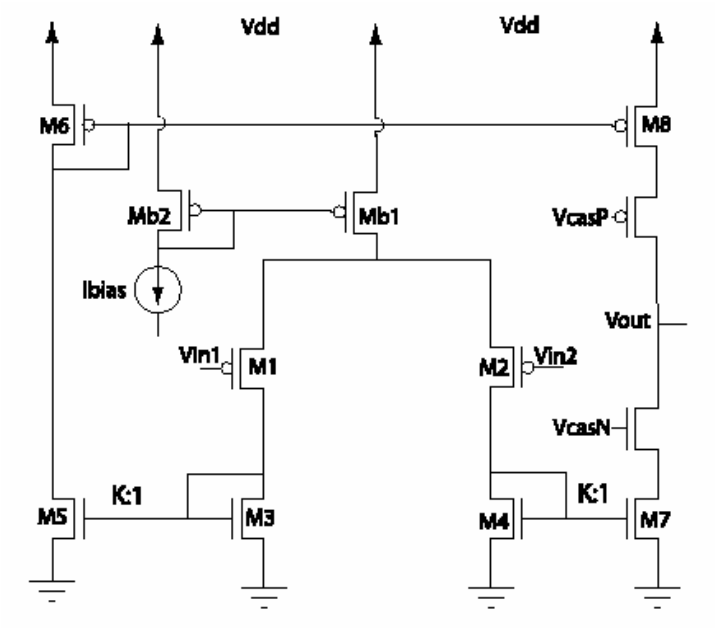

Fig. 4.7 (a) Operational Transconductance Amplifier with cascodes

$$g_{m1} = g_{m2}\,;\; g_{m3} = g_{m4} = g_{m5} = g_{m7}\,;\; g_{m6} = g_{m8}$$

We model the noise sources by flicker and thermal noise [19]. The input referred noise for a MOS transistor is determined by dividing the noise current source between the drain and the source by the g_m of the device.

$$\overline{V_n^2} = \left(\frac{4kT\gamma}{g_m}\right) + \left(\frac{KF * I_D^{AF}}{C_{ox} * f}\right) * \left(\frac{1}{g_m^2}\right) \qquad (9)$$

where kT is thermal energy, g_m is the transconductance of the MOSFET, γ is a constant equal to 1/2 for sub-threshold and 2/3 for above threshold operation, KF is a process-dependent constant on the order of 10-25 V^2F, I_D is the current level and C_{ox} is the gate oxide capacitance per unit area. The first term in Equation (9) corresponds to the thermal noise and the second term to the flicker noise.

Based on our understanding of the noise sources in the OTA, we perform the small signal analysis to determine the transfer function and the total noise at the output. At low frequencies, assuming perfectly matched devices, the input referred noise for the circuit is given by Equation (10):

$$\overline{V_{inOTA}^2} = 2\overline{V_{n1}^2} + 4\left(\frac{g_{m3}}{g_{m1}}\right)^2 \overline{V_{n3}^2} + 2\left(\frac{g_{m6}}{g_{m1}}\right)^2 \overline{V_{n6}^2} + \left(\frac{g_{mN}}{g_{m1}}\right)^2 \overline{V_{nN}^2} + \left(\frac{g_{mP}}{g_{m1}}\right)^2 \overline{V_{nP}^2} \tag{10}$$

In order to minimize the noise level we must maximize g_{m1} and minimize g_{m3}, g_{m5}, g_{mN} and g_{mP}. However we cannot arbitrarily reduce the sizes of M_3 and M_5 because of stability considerations. Reduction in the bias current will help reduce the flicker noise, but at the cost of a reduced slew rate. The bias current and aspect ratios of the different transistors must be chosen to satisfy these conflicting constraints under the available resources (size, power etc.) allocated to the system.

At high frequencies, the parasitic capacitances associated with the devices can no longer be ignored. The gate-source capacitance of each of the MOSFETs and the Miller effect [13] become important factors in the noise analysis. Assuming that the output resistances of the transistors M_7, M_8, M_N and M_P are all equal to r_o, the transfer function for the OTA is calculated as shown in Equation (11).

$$\frac{V_{01}}{V_{in1}} = \frac{-\frac{g_{m1}r_0}{2}}{\left(1 + s\frac{2C_3}{g_{m3}}\right)} * \frac{1}{1 + s\left(\frac{2C_6 + C_{gd7}(1 + \frac{g_{m6}r_0}{2}}{g_{m6}}\right)} * \left(\frac{1 + g_{mP}r_0}{1 + r_0 s C_L}\right)$$

$$\frac{V_{02}}{V_{in2}} = \frac{\frac{g_{m1}r_0}{2}}{1 + \frac{s\left(2C_3 + (1 + \frac{g_{m3}r_0}{2})C_{gd7}\right)}{g_{m3}}} * \left(\frac{1 + g_{mN}r_0}{1 + r_0 s C_L}\right) \tag{11}$$

$$V_0 = V_{01} + V_{02}$$

C_n and C_{gdn} denote the gate to source and the gate to drain capacitance of each transistor.

The noise contribution of each of the device to the total noise is calculated by tracing the path from the input noise source for that device to the output. The noise is shaped by the transfer function for each device.

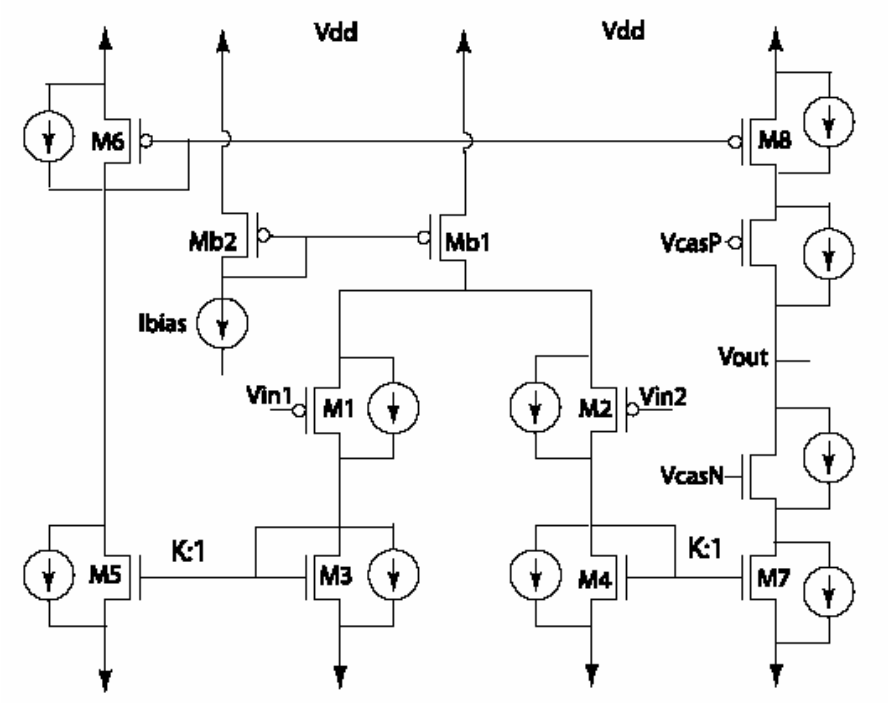

Fig 4.7(b) Noise analysis of OTA. Each device has a noise current source between drain and source.

The region of operation for maximum information transfer rate is simulated using MATLAB [16] .We observe that the spectral region corresponding to the maximum capacity shifts to the higher frequency with increase in the signal power and also the bias current. An increase in bandwidth implies faster changes in the information transfer and hence higher capacity. The capacity or the maximum information that can be transferred by this system increases with the increase in the input power level and also the bias current. This result is in agreement with out theoretical understanding of the inverse dependence of noise on the bias current and the direct

dependence of capacity on the input signal level.

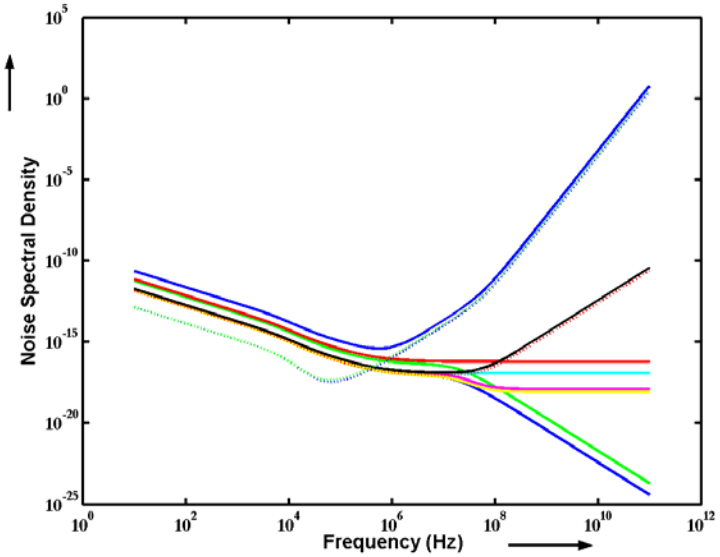

Fig 4.8 Noise contributions of each of the devices in the OTA
M1-green, M2-red, M3-blue, M4-cyan, M5-magenta, M6-yellow, M7-black,
M8-red(:), MN-blue(:), MP-g(:), Total-Blue

We explore different assumptions on the system bandwidth allocation. In one case we fix f1 at 10 Hz, and vary f2 to find the optimal regions of operation for different values f2. As the distribution of the signal shifts to a higher frequency, the signal plus noise level (represented by blue horizontal lines) goes down. For a given signal power constraint the noise is lesser, so we see an increase in the capacity. As f_2 varies from 1 kHz to 10 MHz, we find an increase in information rate by a factor of 104 dB! The optimal region and the variation in the information transfer rates are plotted in Fig4.9. These optimal signal allocations result in the system capacity shown in Fig4.10 reading the frequency axis from left to right. With f1 fixed the capacity increases as we increase f2, and with f2 fixed the capacity increases as we decrease f1. The signal level variation with variation in f1 is not as high as that of that variation with f2. We find the optimal region of operation of this circuit in terms of

information capacity to be around the second pole, which is quite contrary to its regular usage below the first pole!

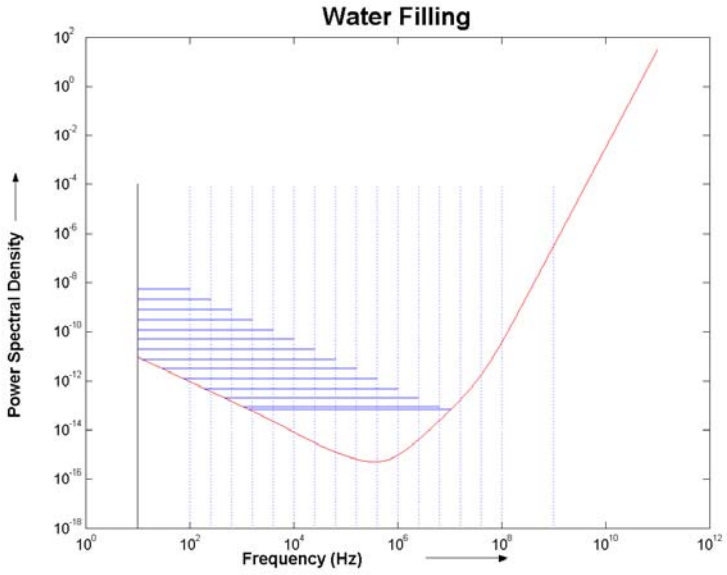

Fig 4.9 Ideal distribution of signal power for constant f1 and varying f2
Horizontal lines represent the signal+noise level and the vertical lines represent brick wall filters.

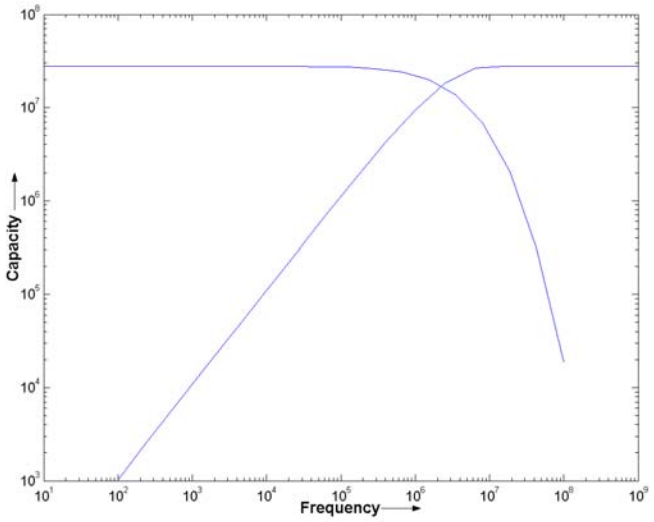

Fig 4.10 Information transfer rates as a function of frequency

Fig 4.11 is a 3-dimensional plot of the maximum transfer rates as a function of bias current and total signal power. Noise is inversely proportional to square root of the

bias current and hence reduces with an increase in the bias current. An increase in signal power causes an increase in the signal-to-noise ratio. Thus capacity increases with an increase in signal power and bias currents.

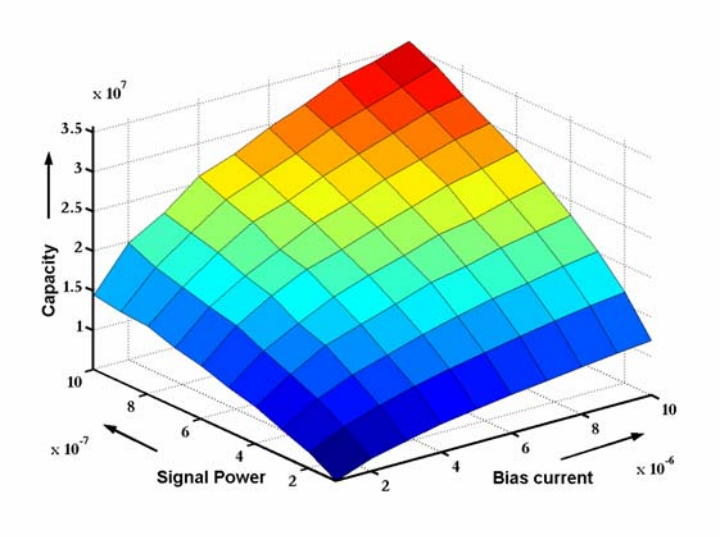

Fig 4.11 Capacity as a function of bias current and signal power
($1\mu A < I_b < 10\mu A$ $\quad$ $1e\text{-}7\ V^2 < P_0 < 1e\text{-}6V^2$)

We assume the crossover point between the sub-threshold and above threshold regions to be current levels of 0.1μA for a square device. Modifying our model to incorporate the sub-threshold behavior by changing the γ in the noise model and the g_m calculation for the device, we compute the capacity of the OTA as a function of signal power and bias current. Fig 4.12 shows that the trend of increasing capacity with increasing bias current and signal power remains unchanged in the sub-threshold region as well.

Our next experiment is to reduce the signal power levels by an order of magnitude from 10e-7 to 10e-8 while keeping the bias current levels same as shown in Fig 4.13.

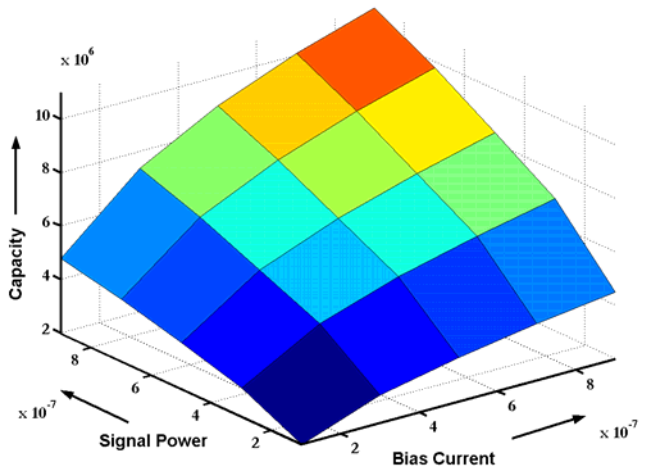

Fig 4.12 Capacity as a function of bias current and signal power

(100nA < I_b <1μA 1e-7 V^2 < P_0 < 1e-6V^2

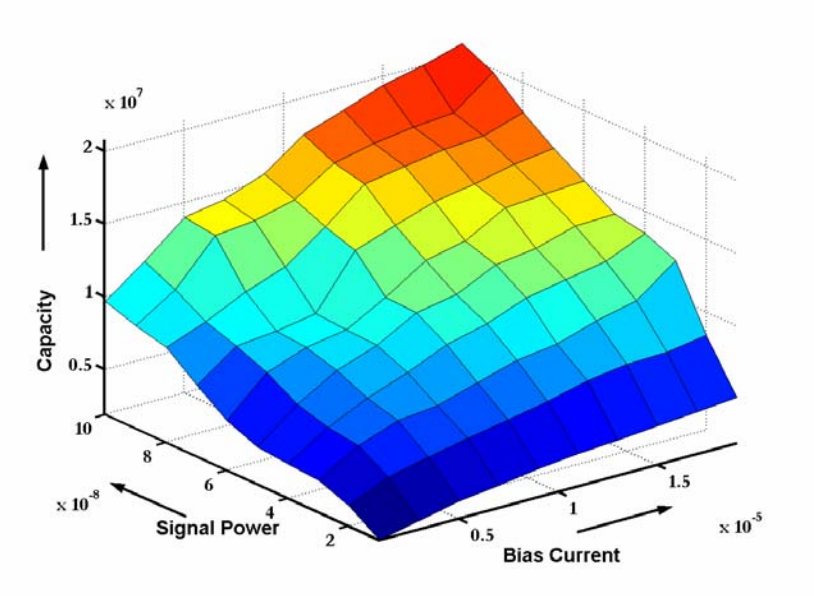

Fig 4.13 Capacity as a function of bias current and signal power

(1μA < I_b <20μA 1e-8 V^2 < P_0 < 1e-7V^2)

We verify that capacity increases with increase in signal power and bias current across a wide spectrum of power levels and current levels. In practical systems power levels less than -50dBm are difficult to discern simply because the environmental noise is higher by almost an order of magnitude. The interesting

regions are current levels between 1nA and 20 μA and power levels between 100 μV and a few mV.

4.3.2 Custom Amplifier

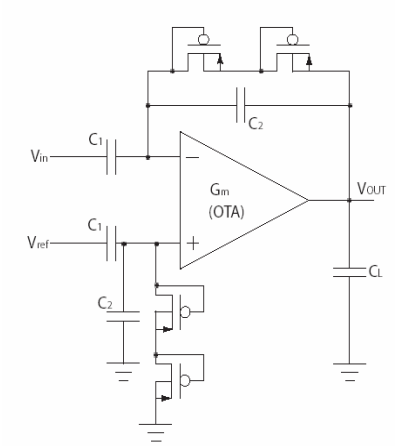

Fig 4.14 Bio-amplifier

We have designed a custom VLSI amplifier based on the OTA discussed in chapter3. This amplifier has been fabricated in a commercially available 0.5μm technology through MOSIS. The amplifier is an OTA in capacitive feedback configuration. This configuration requires a large feedback resistance, which can be achieved using back to back diode connected PMOS devices [9] or using a MOSFET controlled by a bias voltage [10]. For the bio-amplifier design, considering the feedback network consisting of capacitors C_1 and C_2 to be noiseless [9], the input referred noise of the circuit is given as

$$\overline{V_{inAmp}^2} = \left(\frac{C_1 + C_2 + C_{in}}{C_1} \right) * \overline{V_{inOTA}^2} \tag{12}$$

For a typical midband gain of 100, the input referred noise is almost the same as that of the OTA. Therefore, the optimal region of operation of this circuit is close to that of the OTA.

4.4 Experimental Results

The experimental data were collected from the custom amplifier described in the previous section. We made a test fixture with the IC mounted on a vector board. The output of the amplifier feeds into a voltage follower amplifier made from discrete components (Texas Instruments TL074). To prevent environmental noise from affecting the measurements, the vector board was placed in a die cast aluminum box.

Transfer function and noise measurements on the OTA based amplifier were done using the HP 4395A (10Hz – 500 MHz) spectrum/network analyzer. The arrangement is shown in the Fig 4.15. The spectrum /network analyzer was operated in the spectrum analyzer mode and the input to the amplifier was grounded for the noise measurements. The bias current was sourced through a Keithley 236. Our fabricated IC had amplifiers with gains of 20, 40, and 100. We performed the noise measurements for all the amplifiers with bias currents ranging from 10 μA to 20 μA.

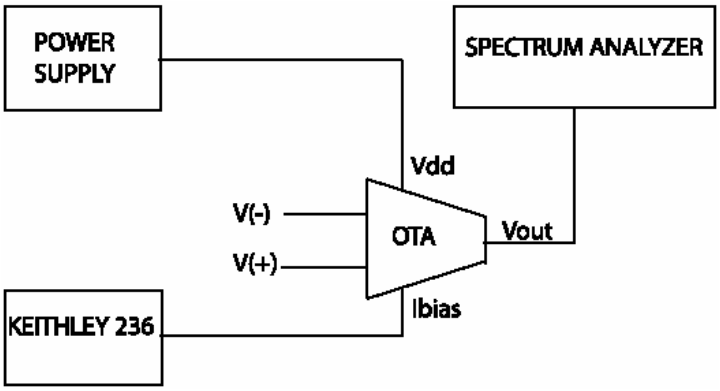

Fig 4.15 (a) Block diagram of measurement set up

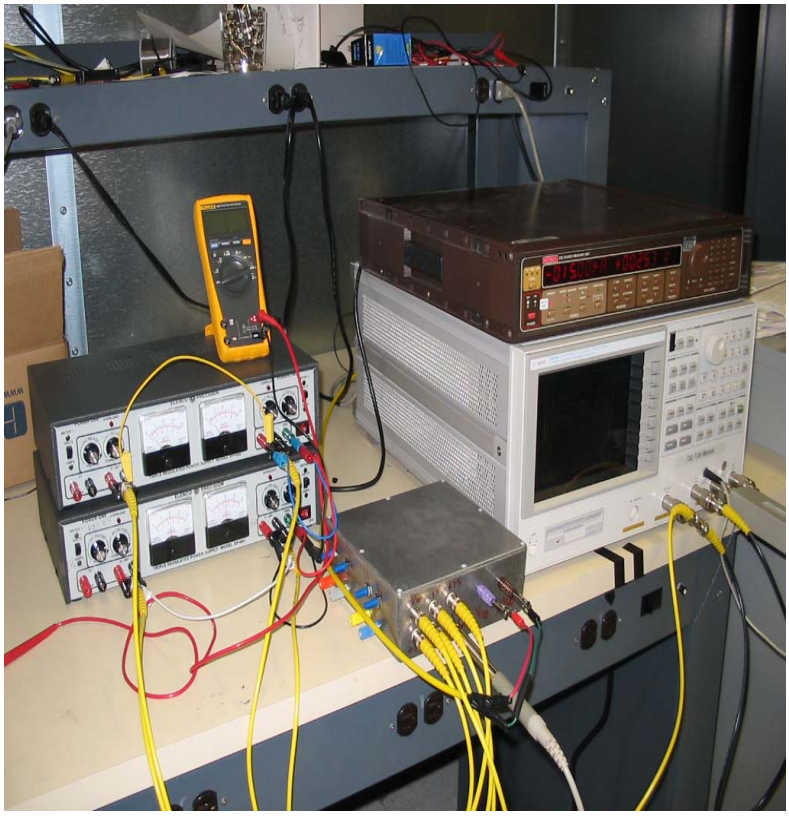

Fig 4.15 (b) Actual set up for measurements

We ground the inputs and measure the noise at the output. Fig 4.16 is the measured noise at the output for the amplifier of gain 100 and different current levels. Notice that at low frequencies the noise is lowest for lowest current (10μA). Next we perform the transfer function measurements. The spectrum analyzer was used in the network analyzer mode and the input was sourced through it. The measured transfer function for gain of 100 and different current levels is shown in Fig 4.17.

The input referred noise is determined by dividing the noise at the output by the transfer function of the circuit. Using numerical methods, we fit the data to the closest curve. The measured and curve fitted data are shown in Fig 4.18

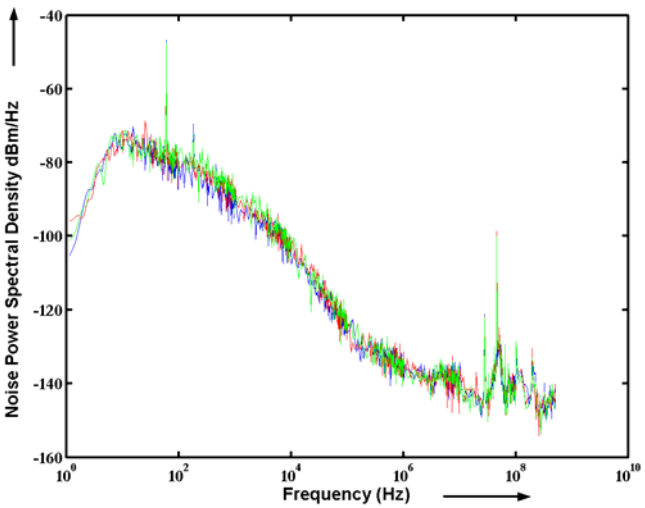

Fig 4.16 Measured noise at the output.
Blue- 10µA, Red - 15µA, Green-20µA

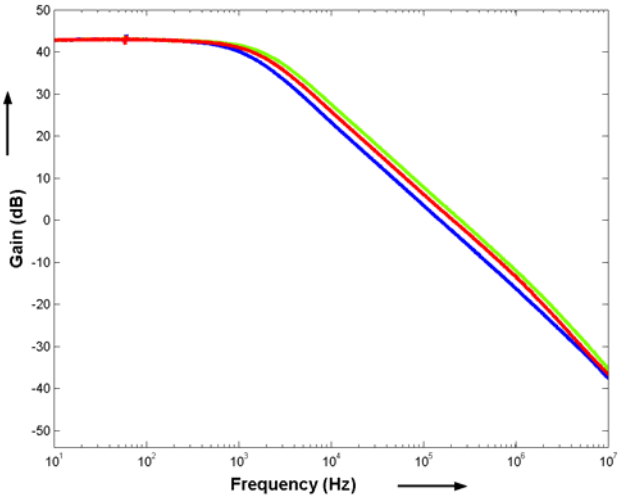

Fig 4.17 Measured transfer functions
Blue- 10µA, Red - 15µA, Green-20µA

The next step is to apply the water filling model to this data. Our circuit's bandwidth is only around 2 kHz for a midband gain of 100. The noise minima is in kHz range. We keep the lower cut off frequency fixed at 100 Hz and shift the higher cut off frequency from 750Hz to 100 kHz. We fix 100 kHz as the upper limit since the gain becomes negligible beyond this frequency.

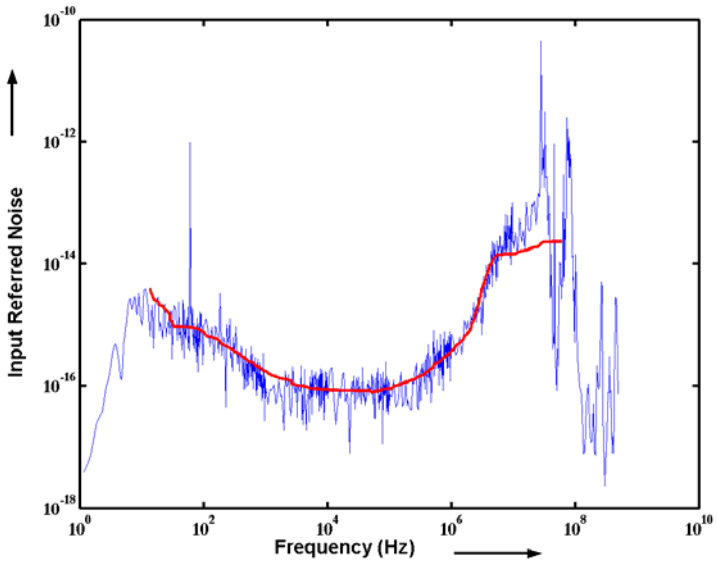

Fig 4.18 Input Referred Noise (blue- actual data, red- curve fitted data) for bias current of 20uA and gain of 40dB

For a given signal power level of 300μV and bias currents of 10μA-20μA , the capacity increases as we shift to the higher frequency ranges as shown in Fig 4.19. This is in compliance with the prediction of our model. We observe from Fig 4.17 that for lower frequencies the noise at the output is lowest for 10μA. The transfer functions are almost the same for all the three currents levels measured as shown in Fig 4.18. As we move to the higher frequencies, the noise at the output is the same for all the currents (Fig 4.17), but the transfer function is highest for current of 20μA (Fig 4.18). This explains why the capacity for 10μA is highest at lower frequencies and for 20 μA is highest at higher frequencies. The cross over point is around 10 kHz.

This is in accordance with the fact that higher currents give more gain, more noise at the output, less input referred noise and hence more capacity but at the cost of higher static power dissipation.

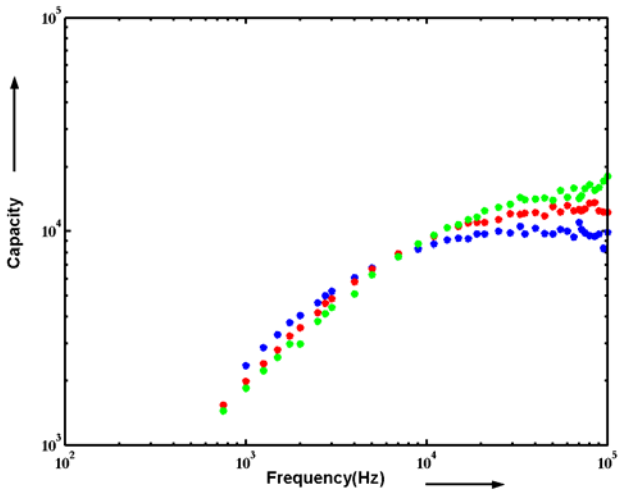

Fig 4.19 Variation of capacity with f2 shifting to higher frequencies.
Blue- 10μA, Red - 15μA, Green-20μA

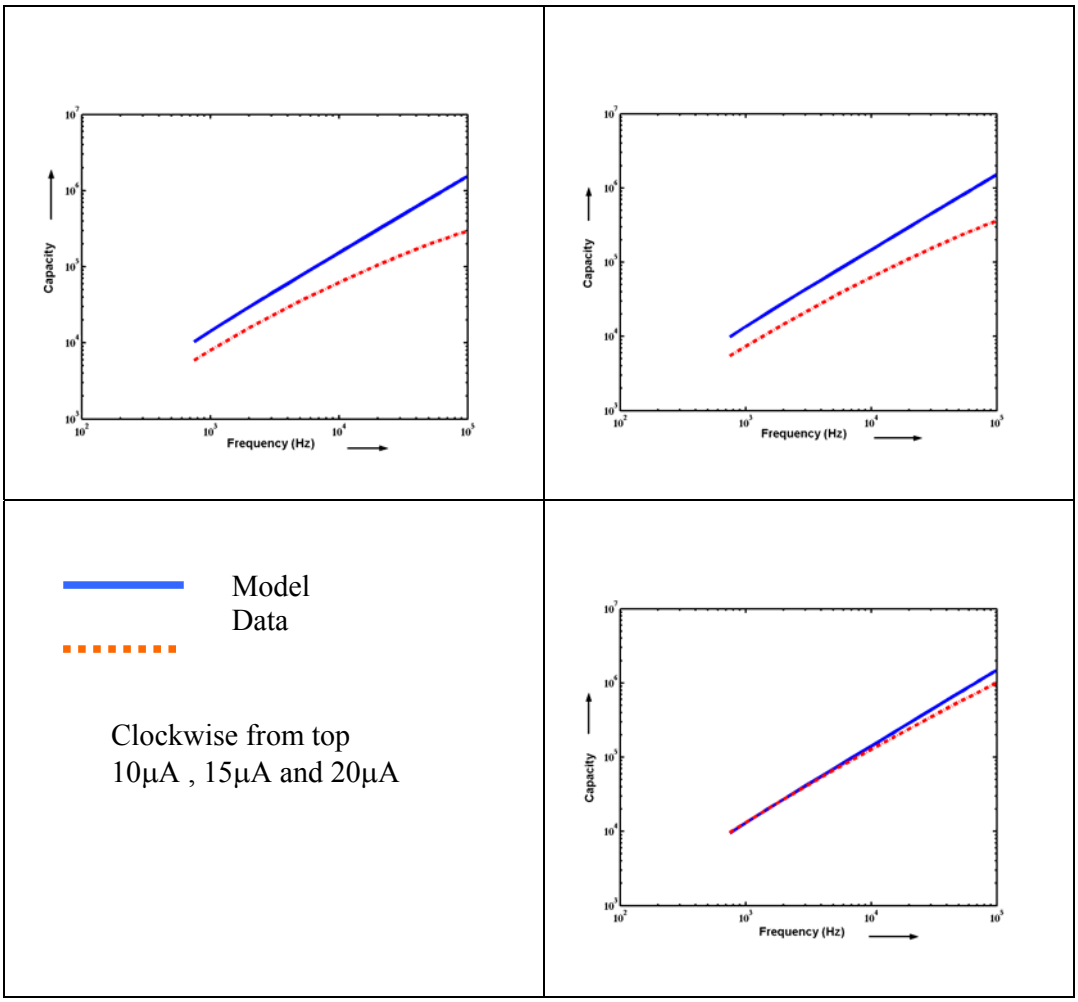

Fig 4.20 Comparison of experimental data with model for capacity variation with changing f2.

4.5 Discussion

We compare the noise predicted by our model to the noise of the OTA device. While there are obvious quantitative differences between the model and the data, there are striking qualitative similarities as shown in Fig 4.20.

The channel capacity given by Equation (2) is an upper bound on the rate of information transmission, assuming that the signal is limited only in average power and the noise is normally distributed. Bandwidth limitations alone do not limit information transmission; a bandwidth limitation which affects signal and noise equally does not affect the channel capacity. Capacity can be increased arbitrarily by increasing the signal power; we must specify how the signal power is constrained such that Equation (2) is meaningful.

4.6 Conclusions

Practical analog systems suffer a reduction in information as a signal propagates through multiple stages of a system. This reduction can be minimized if the system is operated in regions where noise is minimal. This suggests alternate strategies for information-efficient sensing such as signal chopping or modulation at the input stage to transfer information content of the signal to a higher frequency for optimal use of the circuit as an information channel.

Noise limits information transmission in practical analog systems and sets lower bound on power. Water-filling algorithm gives efficient distribution of signal power in a noisy channel. Given noise and transfer characteristics we compute optimal information rates for the linearized OTA. This also specifies the most efficient way to use the channel. We conclude that operating the OTA at higher frequency where the noise is less increases the capacity of the system considerably.

Chapter 5

Bit-Energy

The minimum cost incurred by the transmission of one bit of information through the channel is a fundamental figure of merit characterizing the most economical way to communicate reliably. Its reciprocal, the capacity per unit cost, is defined similar to the conventional capacity, except that the ratio of the logarithm of the number of the codewords to their block length (rate) is replaced by the ratio of the logarithm of the number of codewords to the their cost (rate per unit cost).

As shown by Verdu [24], the capacity per unit cost can be computed from the capacity – cost function by finding $\sup_{\beta>0} C(\beta)/\beta$, or alternatively, as

$$C = \sup_{X} \frac{I(X;Y)}{E[b[X]]} \tag{1}$$

For any system with a power constraint the capacity is a measure of the maximum information transfer rate between the input and output [2]. This holds if we consider our system as a zero cost system i.e. we say that there is no cost involved in achieving these rates. But in the real world there is a price for everything. We introduce this cost in our analysis. The bit-energy gives the minimum power required to transmit a single bit of information through the system; it provides an appropriate standard for comparing the efficiency of communication among different technologies. Besides the power constraint

on the input of a system, there is an implicit cost i.e. the static power dissipation required by the system to operate. For the OTA it is a function of the bias currents and voltage requirements of the circuit.

We compute the capacity per unit power of input signal ($\frac{C}{P_{sig}}$) and the capacity per unit total power budget of the system i.e. the sum of power constraint on the input signal and the static power dissipation ($\frac{C}{P_{sig}+P_{STATIC}}$). It is important to note here that our capacity analysis has the both these power constraints built in. The dependence of the input referred noise on the bias current level introduces the static power dissipation and the signal to noise ratio has the input power constraint.

5.1 Capacity per unit signal power

Capacity is computed as $C=\log\left(1+\frac{P_{sig}}{N}\right)*F$ where P_{sig} is the signal power constraint, N is the noise spectral density and F is the bandwidth.

$\frac{C}{P_{sig}}$ is the capacity per unit signal power . It is the actual cost in terms of signal power for maximum information transfer; $\frac{C}{P_{sig}}=\max\frac{I(X;Y)}{P_{sig}}$. This sets the limits on the signal power for achieving the maximum capacity. The maximum information transfer rate is determined by the water filling approach and is a function of P_{sig} and the I_{bias}. So our actual cost metric is $\frac{C(P_{sig},I_{bias})}{P_{sig}}$. As the noise power reduces with the increase in bias current, the capacity per unit power goes up asymptotically as a logarithmic function of

bias current. As the signal power is increased, the capacity per unit signal power goes down as a logarithmic function of signal power. This is shown in Fig 5.1.

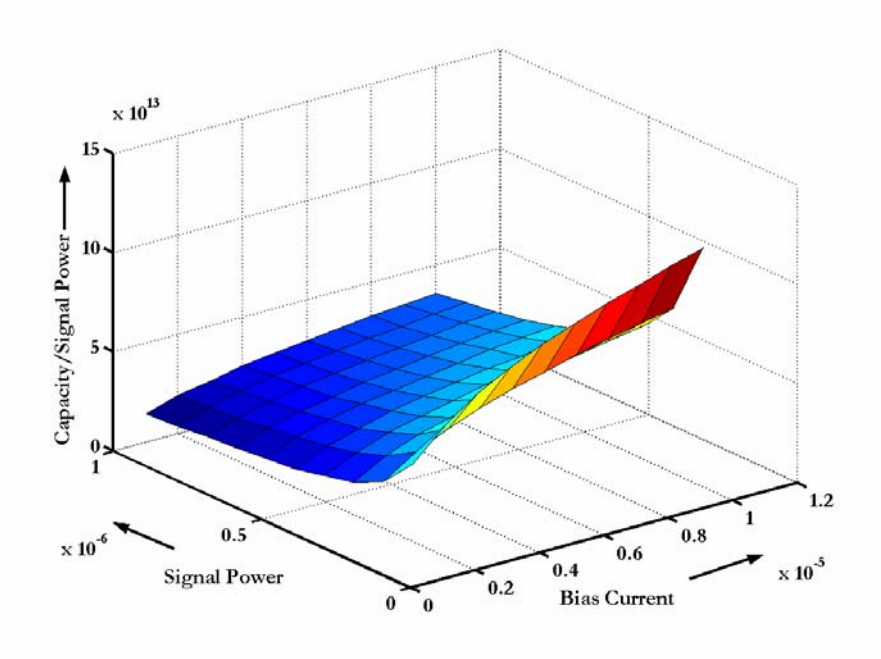

Fig 5.1 Capacity per unit Signal Power

5.2 Capacity per unit total power

If we want to quantify the total power constraint for the system, we should also take into account the power needed to bias the system i.e. the static power dissipation. The static power dissipation is determined by the total power needed to operate the system and the biasing level. For the OTA it is given as $P_{static} = V_{dd} * I_{bias} * (2 + K)$ where, K is the current mirror gain factor.

Our metric now is $\frac{C(P_{sig}, I_{bias})}{P_{sig} + P_{static}}$ where $P_{sig} + P_{static}$ is the total power budget of the system. As we increase the signal power keeping the current level fixed, we notice an increase in the capacity per unit total power. Alternatively, as we increase the bias current keeping the signal power constant, the capacity per unit power decreases.

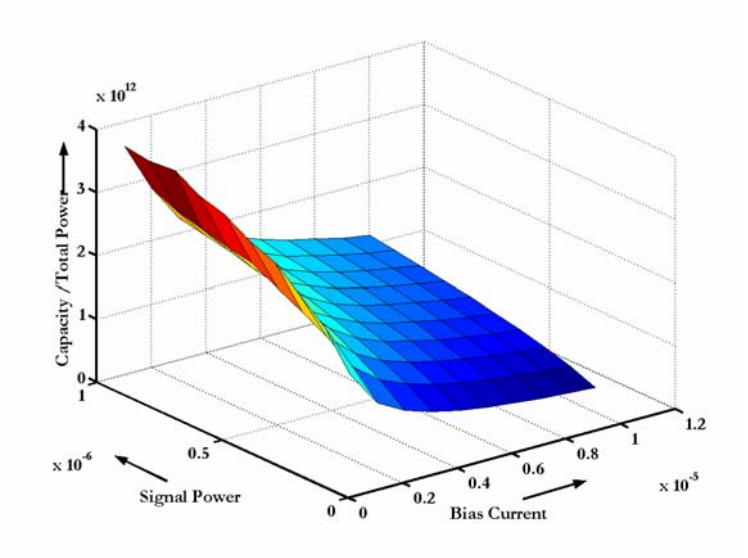

Fig 5.2 Capacity per unit Total Power

5.3 Conclusions

I_{bias} , P_{sig}	**Capacity**	**Capacity/P_{sig}**	**Capacity/P_{sig}+P_{static}**
I_{bias} increases, P_{sig} constant	Increases	Increases	Decreases
P_{sig} increases, I_{bias} constant	Increases	Decreases	Increases
Simulations	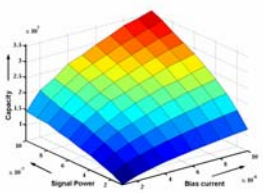	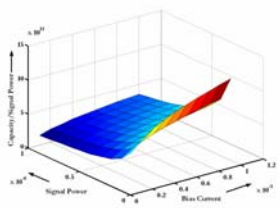	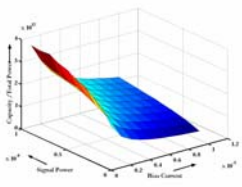

Fig 5.3 Variation of Capacity Metrics with Power constraints

The analysis for maximum capacity has been extended to cover the cost incurred in achieving that capacity. An increase in bias current reduces the noise and hence increases

the capacity but at the cost of higher static power dissipation. An increase in the power content of the signal increases the capacity.

The given power budget is the deciding factor. If there is a constraint on the input signal power level, increase the bias current to increase capacity. Alternatively, if there is a constraint on the maximum power available to the circuit for operation then signal power has to be boosted for improving the capacity.

Chapter 6

Noise Efficiency Factor

Noise is a limiting factor in improving the capacity of a system. Steyaert *et al* [23] proposed a metric for comparing the noise performance of analog amplifiers called the Noise Efficiency Factor (NEF). The noise performance of the circuit is compared to the noise performance of a simple bipolar transistor considering only thermal noise and no base resistance [13]. In line with the definition of NEF, we determine the capacity of a bipolar transistor (C_{NEF}). Next, we compute the capacity of OTA (C_{OTA}) considering only thermal noise [9] since it is the dominant noise source in the circuit and compare it with that of the bipolar transistor.

6.1 Noise Efficiency Factor for a bipolar transistor

The NEF of the system is defined as the ratio of total input referred noise of the circuit to the total input referred noise of the bipolar transistor. The NEF describes how many times the noise of a given system with the same drain current and bandwidth is higher compared to the ideal case of a simple bipolar transistor. The total equivalent input noise of an ideal bipolar transistor (only thermal noise and no base resistance) is given by [13]

$$V_{rms,in} = \sqrt{BW * \frac{\pi}{2} * \frac{4 * k * T}{gm}} = \sqrt{BW * \frac{\pi}{2} * \frac{4 * kT * U_T}{I_C}} \quad (1)$$

where, BW for the bipolar transistor this is the unity gain bandwidth f_t.

The definition of NEF simplifies to,

$$NEF = V_{rms,in} \sqrt{\frac{2 * I_{tot}}{\pi * U_T * 4kT * BW}} \quad (2)$$

where, I_{tot} is the total drain current in the system and $V_{rms,in}$ is the total equivalent input noise of the circuit.

The total thermal noise for the OTA circuit is given as [9]

$$\overline{V^2_{thermal,in}} = \left[\frac{16kT}{3g_{m1}} \left(1 + 2\frac{g_{m3}}{g_{m1}} + \frac{g_{m7}}{g_{m1}} \right) \right] \Delta f \quad (3)$$

Substituting (3) in (2) and with g_{m3}, $g_{m7} << g_{m1,}$ we find

$$NEF = \sqrt{\frac{4I_{tot}}{3U_T g_{m1}}} = \sqrt{\frac{16}{3U_T} \left(\frac{I_{D1}}{g_{m1}} \right)} \quad (4)$$

where, I_{D1} is the drain current through M_1 which is ¼ of the total amplifier supply current.

6.2 Capacity of BJT and OTA

The capacity for a continuous band limited system is given by [22]

$$C = BW * \log\left(1 + \frac{P_{sig}}{V_{in}^2} \right) \quad (5)$$

For a bipolar transistor BW = $f_t = \frac{g_m}{2\pi(C_\mu + C_\pi)}$ (6)

Substituting $V_{rms,in}$ from (1) and BW from (6) in (5) we get

$$C = \frac{I_{bias}}{2\pi U_T (C_\mu + C_\pi)} \log\left[1 + \frac{P_{sig}(C_\mu + C_\pi)}{2kT}\right] \tag{7}$$

We compute the capacity as a function of signal power and bias currents as shown in Fig 6.1 and the capacity of the OTA with only thermal noise and without applying the water filling optimization as shown in Fig 6.2.

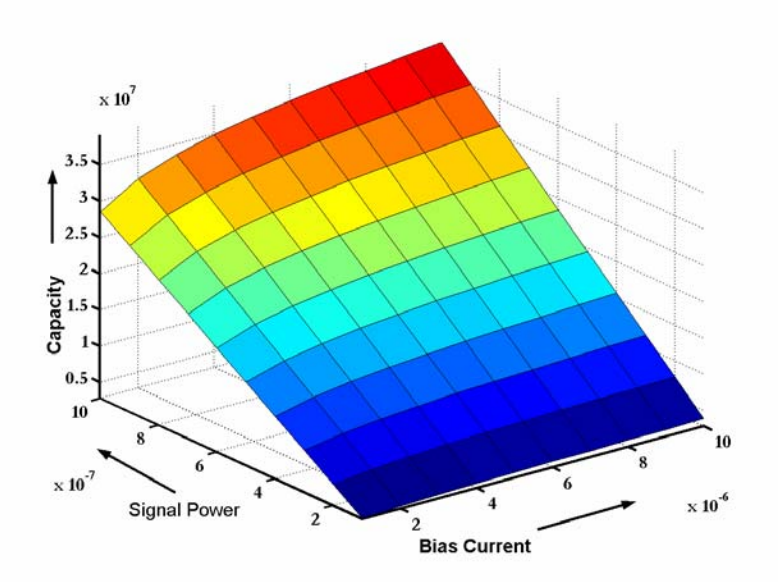

Fig 6.1 Capacity of a simple Bipolar Transistor

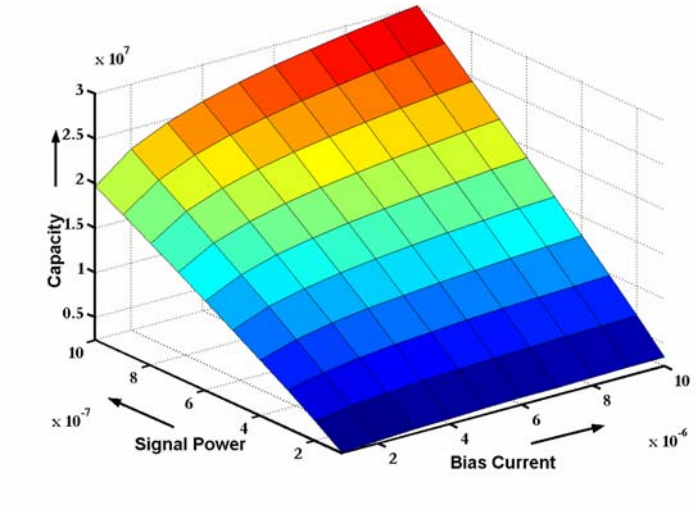

Fig 6.2 Capacity of OTA with Thermal noise

6.3 Conclusion

The capacity of the BJT and the OTA under similar constraints of bandwidth and total current, are plotted on the same scale in Fig 6.3. Since the noise performance of the BJT is better than the OTA, the capacity of the BJT is higher than the capacity of the OTA. This is very evident from Fig 6.3.

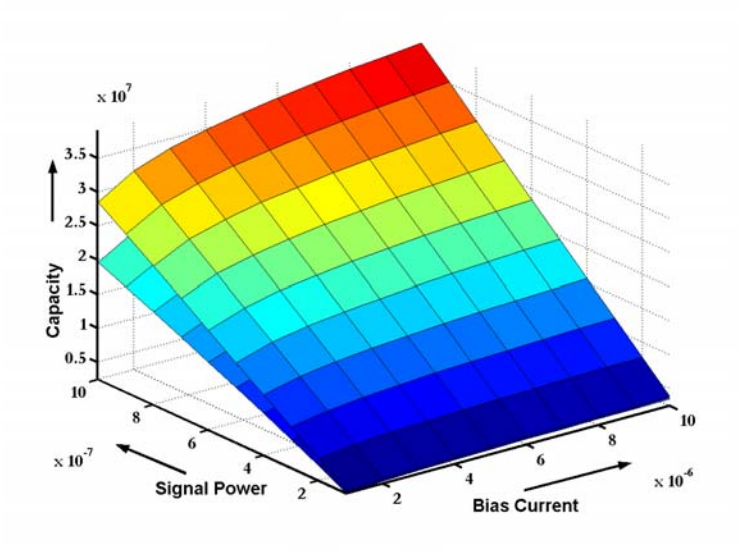

Fig 6.3 Capacity of BJT and Capacity of OTA as a function of signal power and bias current. The upper surface is the BJT and the lower surface is the OTA.

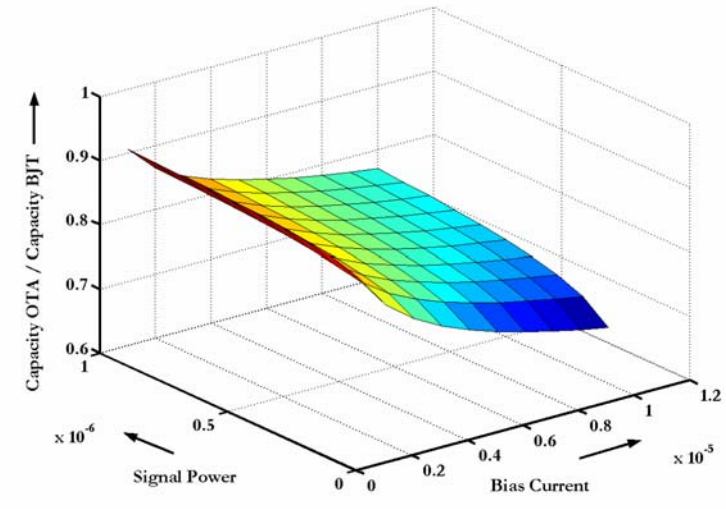

Fig 6.4 C_{OTA}/C_{BJT} as a function of bias current and signal power

Fig 6.4 shows how the ratio of the capacities of the OTA and BJT vary with changing signal power and current levels. As we increase the signal power, the capacity of the OTA increases faster than the capacity of the BJT. Increasing the bias current shows the reverse trend; the capacity of the OTA reduces slower than the capacity of the BJT.

We can conclude that at lower current levels, the capacity of the OTA will be closer to the capacity of the BJT. In other words, to achieve the noise performance of the BJT, we need to reduce the bias current and shift the operation in the sub-threshold domain. This is in agreement with the NEF comparison of OTA with BJT in [9]. Operating some of the devices in OTA in the sub–threshold region is one way of improving the noise performance of the system.

Chapter 7

Conclusion

The focus of this work is to investigate the information efficiency of an OTA based amplification system. We apply principles of information theory to analog circuits in an effort to optimize their performance. The specific application is to design efficient sensor systems for neural recordings that are able to transfer maximum information between input and output. We start with treating the amplifier system as a channel for transmitting information. We model the system as a Gaussian channel with power constrained input signal and corruption due to noise and determine the capacity of the system.

Chapter 1 describes the experiments to record the electrical activity of living cells. These experiments give us the actual power content of the electrical signals that we get from the cells. We aim to design amplifiers according to the measured spike spectrum and power levels. In Chapter 3 we describe the OTA circuit and the various characterization parameters. We introduce the noise sources and discuss their representation in a circuit. Chapter 4 presents a detailed description of the analytical model for determining the information capacity of the OTA. We employ the water filling algorithm to determine the spectral region where the capacity can be maximized. Capacity increases with increasing bias current and signal power levels. As we shift the

bandwidth allocation to the higher frequencies where noise is minimal, there is an increase in capacity. We measure the noise at the output and the transfer function from the fabricated device. We apply our model to the actual data and perform comparisons between the results from the data and the model. We observe that the measurements follow the trend the model predicts; at higher frequencies where noise is minimal, capacity of the system is increased. In chapter 5, we introduce power efficiency in our analysis. The cost for achieving the desired capacity is two-fold; the power constraint on the signal and the static power dissipation in the circuit. We contrast capacity per unit signal power with the capacity per unit total power. Noise efficiency factor has been used to compare the noise performance of amplifiers. A simple bipolar transistor has the lowest NEF. We compute the capacity of a bipolar transistor under the same power constraints and similar biasing requirements as our circuit. Operating the circuits at lower current levels reduces the gap between the noise performance of the OTA and the bipolar transistor.

This work is the first step towards maximizing the information transfer in amplifier systems for neural recordings. Applying principles of information theory to characterize the system as a channel, we determine the channel capacity of the OTA. This approach can be developed into an engineering design tool for designing efficient systems. This analysis provides us information about the frequency bandwidth for signal allocation, the cost in terms of signal power constraint as well as the static power and bias current levels for reducing the noise in the system.

7.1 Future Work

7.1.1 Encoding/Decoding Scheme

The findings of this analysis are quite contrary to the regular designs of amplification and filtering circuits. These amplifiers are usually operated at frequencies near their first pole. But to get maximum capacity, they should be operated at much higher frequencies. These frequencies might be outside the useful bandwidth of these amplifiers. This brings up another challenging area of research. Is it feasible to operate these amplifiers at these higher frequencies? If we could shift the spectral content of the signal to the higher frequency without affecting the noise spectral density distribution then we could achieve higher signal to noise ratios. In the case where the spectral content of the signal cannot be varied then even a shift to the frequency range where noise level is a minimum gives rise to an increase in SNR leading to an increase in the information transfer rate. The cost involved in this process is the reduction in the gain of the system. Fig 7.1 is an illustration of this observation.

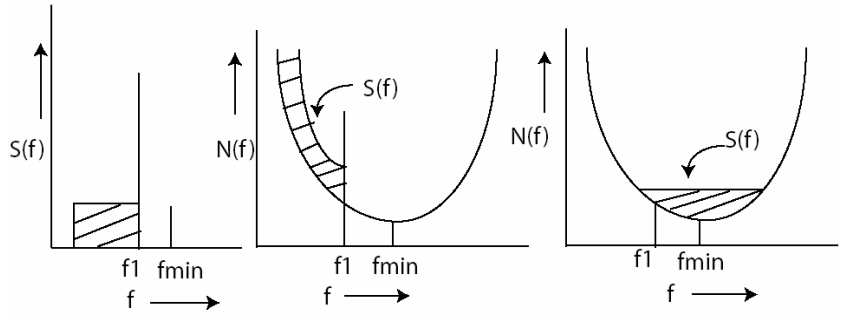

(a) (b) (c)

Fig 7.1 (a) A system with input signal whose frequency spectrum cannot be altered (b) System used for maximum gain (c) System used for maximum capacity

This puts forth the need for an encoding/decoding scheme to shift the input signal to a higher spectrum and reconstruct the original signal at the output. The over-head involved in introducing these intermediate stages in terms of power requirement and the noise performance has to be carefully analyzed.

7.1.2 Range of the Analytical Model

In chapter 4 we present results for the capacity computation for the OTA for the above threshold and below threshold operation. There is a discontinuity in this crossover as seen is Fig 7.2, since our model uses different parameters in the above threshold and sub threshold case. To better understand and determine the effect of subthreshold and above threshold operation, we need to have a continuous model applicable to both regions.

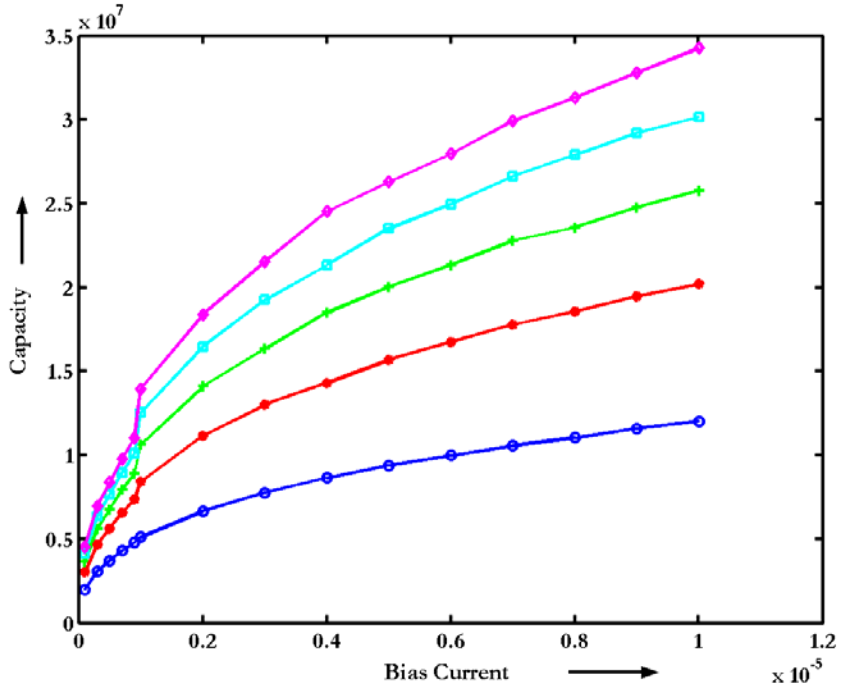

Fig7.2 Crossover between sub-threshold and above threshold. The first 5 points are subthreshold and the next 10 points are above threshold

My study of efficient communication has been primarily limited to fundamental noise sources. In different contexts, however, what we mean by "noise" and "signal" changes, and in many applications the dominant noise sources are practical rather than fundamental. These practical noise sources must be characterized empirically, and included in the analysis.

The focus of this work has been the quantification of information and information–power efficiency for Operational Transconductance Amplifier. I chose channel capacity and bit-energy as performance measures for this research. While these measures are fundamental and physically-motivated, they are not representative of all design constraints and tradeoffs, and further work is necessary to transition this approach into a practical design tool.

Bibliography

[1] Milton Abramowitz and Irene A. Stegun, editors. *Handbook of Mathematical Functions With Formulas, Graphs, and Mathematical Tables*. US Department of Commerce National Bureau of Standards, 1964.

[2] Pamela A. Abshire. *Sensory Information Processing under Physical Constraints.* PhD thesis, Johns Hopkins University, 2001.

[3] R. Baker, H. Li, and D. Boyce, *CMOS Circuit Design, Layout, and Simulation,* New York: IEEE Press, 1st ed., 1997, Pages: 617-679.

[4] Thomas M. Cover and Joy A. Thomas. *Elements of Information Theory*. JohnWiley & Sons, Inc., New York, 1991.

[5] C.C.Enz. The Theory of Semiconductor Noise and the Principles of Low-Noise Design. *EPFL*, May16,1993.

[6] P.M. Furth and A.G. Andreou. Comparing the bit-energy of continuous and discrete signal representations. In *Proceedings of the Fourth Workshop on Physics and Computation (PhysComp96)*, pages 127–133, Boston MA, November 1996. New England Complex Systems Institute.

[7] Paul . R. Gray, Paul J. Hurst, Stephan Lewis and Robert G. Meyer. *Analysis and Design of Analog Integrated Circuits.* Fourth Edition, John Wiley and Sons Inc 2001.

[8] C González and M Rodríguez. A flexible perforated microelectrode array probe for action potential recording in nerve and muscle tissues. *Journal of Neuroscience. Methods.* 72, 189-195, (1997).

[9] Reid R. Harrison and Cameron Charles. A Low-Power Low- Noise CMOS Amplifier for Neural Recording Applications. *IEEE Journal of Solid-State Circuits,* vol.38, no.6: 958-965, June 2003.

[10] T.Horiuchi, T.Swindell, D.Sander and P. Abshire. A Low-Power CMOS Neural Amplifier with Amplitude Measurements for Spike Sorting. Submitted to *IEEE Internaltional Symposium on Circuits and Systems,* May 2004.

[11] Michael L Holmes. *Application of Local Common Mode Feedback Techniques to Enhance Slew Rate and Gain Bandwidth in CMOS Operational Amplifiers.* MS Thesis. New Mexico State University, 2002.

[12] Bedrich J. Hosticka. Performance comparison of analog and digital circuits. *Proc. IEEE*, 73(1):25–29, Jan 1985.

[13] Kenneth R. Laker and Willy M. C. Sansen, *Design of analog integrated circuits and systems*, McGraw-Hill, Singapore, 1994.

[14] Irwin B Levitan and Leonard K Kaczmarek. *The Neuron .Cell and Molecular Biology.* Third Edition. Oxford University Press 2002.

[15] Makeswaran Loganathan, Suvarcha Malhotra and Pamela Abshire. Information Capacity and Power Efficiency of Operational Transconductor Amplifiers. Submitted to *IEEE International Symposium on Circuits and Systems, 2004.*

[16] MATLAB is a registered trademark of The MathWorks, Inc. For MATLAB product information, please contact: The MathWorks, Inc., 24 Prime Park Way, Natick,

MA, 01760-1500, USA. Tel.: 508-647-7000; Fax: 508-647-7001; E-mail: info@mathworks.com; Web: http://www.mathworks.com.

[17] C.D. Motchenbacher and J.A. Connelly, *Low Noise Electronic System Design,* John-Wiley and Sons, New York, 1993.

[18] W. Nisch, J.Böck, U. Egert, H. Hämmerle and A. Mohr. A thin film microelectrode array for monitoring extracellular neuronal activity *in vitro*. *Biosensors and Bioelectronics.* **9**, 737-741, 1994.

[19] B. Razavi, *Design of Analog CMOS Integrated Circuits,* New York: McGraw-Hill, 1st ed., 2001.

[20] N.Reeves, S.Malhotra, M.Loganathan, JM Lauenstein, J. Chaiyupatumpa, P.Abshire, Y.Liu, E.Smela. Integrated MEMS structure and CMOS circuits for bioelectronic interface with single cells. Submitted to *IEEE International Symposium on Circuits and Systems, 2004.*

[21] N. R. Shanbhag. A mathematical basis for power-reduction in digital VLSI systems. *IEEE Transactions on Circuits and Systems part II: Analog and Digital Signal Processing*, 44:935–951, 1997.

[22] Claude E. Shannon. Communication in the presence of noise. *Proceedings of the I. R. E.*, 37:10–21, Jan 1949.

[23] Micheal J. Steyaert, Willy M.Sanson and Chang Zhongyuan. A Micropower Low-Noise Monolithic Instrumentation Amplifier for Medical Purposes. *IEEE Journal of Solid-State Circuits,* vol.22, no.6: 1163-1168, December 1987.

[24] S. Verdu. On Channel Capacity per unit Cost. *IEEE Trans. Inform. Theory,* 36:1019-1030, September 1990.

[25] R. H. Whittington, K.H. Gilchrist, L.Giovangrandi and G.T. A. Kovacs. A Multi-Parameter, Feedback-Based Electrical Stimulation System for Cardiomyocyte Cultures. *International Conference on Solid State Sensors, Actuators and Microsystems,* June 2003.

[26] B.C. Wheeler and J.L. Novak. *IEEE Transactions on Biomedical Engineering*.BME -33(12): 1204-12, 1986.